Nonlinear Dyn
https://doi.org/10.1007/s11071-024-10443-y

RESEARCH

On the dynamics of transporting rolling cylinders

Theresa E. Honein · Oliver M. O'Reilly

Received: 20 May 2024 / Accepted: 29 September 2024

Abstract A common, yet hazardous, method of transporting cylindrical tanks used to carry compressed gas involves rolling both tanks at opposite angles of inclination to the vertical. By propelling one of the tanks while maintaining point contact between the tanks, both tanks can be moved such that their centers of mass move in a straight line. The purpose of this paper is to explore this locomotion mechanism. First, the problem of supporting an inclined cylinder in point contact with a rough surface is examined. The analysis shows that dependent on the geometry of the cylinder and the coefficient of static friction, a wide range of angles of inclination are feasible. The presence of non-integrable constraints on the motion of the rolling cylinder is explored using the concept of a holonomy. The problem of transporting two cylinders using the aforementioned mechanism is then analyzed with the help of Frobenius' integrability criterion for constraints and numerical simulations. The results show the mechanical advantage of transporting a pair of cylinders, the range of possible angles of inclination, and the forces needed to sustain the motion.

Keywords Rigid body dynamics · Non-holonomic constraints · Holonomy · Locomotion

T. E. Honein · O. M. O'Reilly (✉)
Department of Mechanical Engineering, University of California, Berkeley, CA 94720-1750, USA
e-mail: oreilly@berkeley.edu

T. E. Honein
e-mail: theresa_honein@berkeley.edu

1 Introduction

A common, yet hazardous, method of transporting two cylindrical tanks used to carry compressed gas involves rolling both tanks at opposite angles of inclination to the vertical (cf. Fig. 1).[1] By propelling one of the tanks while maintaining point contact between the tanks, both tanks can be transported together with their centers of mass moving in straight lines. Apart from safety concerns, this mechanism for transporting tanks also raises questions about the dynamics of the cylinders involved. For instance, is there rolling or sliding contact at the point of contact between the cylinders, what is the range of feasible angles of inclination, and is it necessary to support the entire weight of both cylinders?

To explore the dynamics of the locomotion mechanism, we are able to leverage the wealth of research on rolling cylinders in the literature. Much of this work can be traced to seminal papers by Appell [1] and Korteweg [2] on the rolling disk in the early 1900 s and the large numbers of recent papers (cf. e.g., [3–6]) that were inspired by the paradoxical behavior of a cylinder of chrome plated cast iron known as Euler's Disk.

We start our analysis with a exploration of the problem of supporting an inclined cylinder that has a single point in contact with a rough surface and is supported by an applied force at the other end of the cylinder (cf. Sect. 2). As the contact condition is maintained by

[1] A demonstrative example can be found here:https://youtu.be/Vgn5fv__LAk.

Published online: 05 November 2024

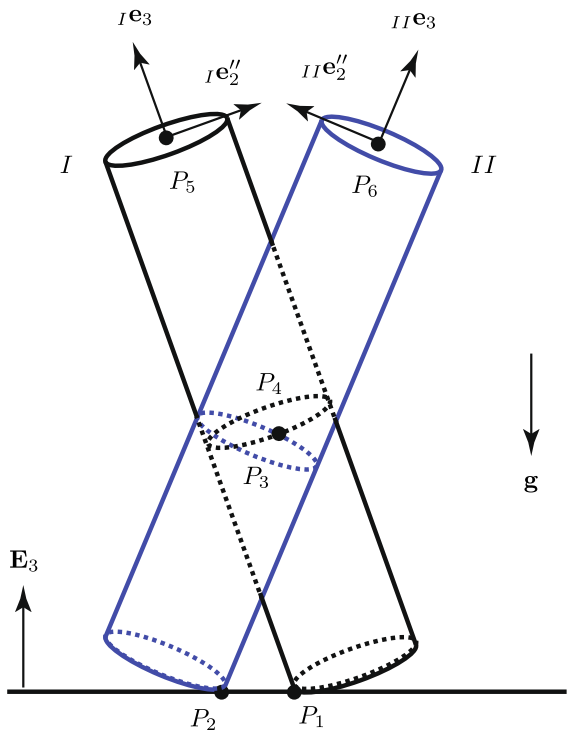

Fig. 1 A pair of cylinders in motion on a horizontal surface. Each cylinder has a single point of contact with the surface and a single point of mutual contact

a static friction force, in Sect. 3 we show that multiple equilibrium configurations and a range of applied forces are feasible. As an alternative to showing that the constraints on the rolling cylinder are non-integrable, we instead leverage the works of [7–9] and explore the holonomy of the rolling cylinder. With these two preliminary studies completed, we then turn to exploring the dynamics of a pair of cylinders in contact at a single point moving in unison on rough horizontal surface. With the help of Frobenius' theorem on integrability of a system of constraints [10,11], we argue that the point contact is one of slipping. With the help of a recently developed numerical method by Capobianco et al. [12], a numerical simulation of the locomotion mechanism is then developed. Our numerical simulations show that the normal force between the cylinders is negligible. Consequently, the results on the forces developed in Sect. 2) on the external forces needed to maintain a cylinder in motion at a given angle of inclination are applicable to each of the pair of cylinders.

Relevant background on rigid body dynamics can be found in the textbooks [10,11] and Shuster's review article [13] on rotations. We follow the notation used in [10].

2 A rolling cylinder

We consider a homogeneous circular cylinder of mass m, height h, and radius r. The position vector of the center of mass $\bar{X}$ is denoted by $\bar{\mathbf{x}}$ and the position vector of the instantaneous point of contact P is denoted by $\mathbf{x}_P$:

$$\bar{\mathbf{x}} = x_1\mathbf{E}_1 + x_2\mathbf{E}_2 + x_3\mathbf{E}_3 \tag{2.1}$$

where $\{\mathbf{e}_1, \mathbf{e}_2, \mathbf{e}_3\}$ is a right-handed set of Cartesian basis vectors for $\mathbb{E}^3$. The position vector of P relative to $\bar{X}$ is denoted by $\boldsymbol{\pi}_P$.

To parameterize the rotation tensor $\mathbf{Q}$ of the cylinder a set of 3-1-3 Euler angles, ψ, ϑ, and φ, are used. The angles define the orientation of a basis $\{\mathbf{e}_1, \mathbf{e}_2, \mathbf{e}_3\}$ that corotates with the cylinder with respect to the basis $\{\mathbf{E}_1, \mathbf{E}_2, \mathbf{E}_3\}$: $\mathbf{Q} = \mathbf{e}_1 \otimes \mathbf{E}_1 + \mathbf{e}_2 \otimes \mathbf{E}_2 + \mathbf{e}_3 \otimes \mathbf{E}_3$. Here, $\otimes$ is the tensor product of two vectors. While the first and third Euler angles range from 0 to 2π, the second Euler angle, $\vartheta \in (0, \pi)$ in order to avoid a coordinate singularity associated with the Euler angle parameterization of a rotation tensor [14]. Referring to Fig. 2, we observe that ϑ is a measure of the inclination of the cylinder to the vertical: when $\vartheta = 0$, the cylinder is vertical and when $\vartheta = \frac{\pi}{2}$ the cylinder is horizontal. In both of these cases, the assumption of a single point of contact that we employ fails. Consequently, for our analyses we assume $\vartheta \in \left(0, \frac{\pi}{2}\right)$ unless otherwise stated. For additional details on the 3-1-3 Euler angles, including several equivalent representations (A5) for the angular velocity vector $\boldsymbol{\omega}$, the reader is referred to Appendix A.

The constraints that the cylinder rolls without slipping on the horizontal surface can be expressed in terms of the velocity vector of the instantaneous point of contact: $\mathbf{v}_P = \mathbf{0}$. As $\mathbf{v}_P = \bar{\mathbf{v}} + \boldsymbol{\omega} \times \boldsymbol{\pi}_P$, the constraints can be expressed as

$$\Pi_1 = 0, \qquad \Pi_2 = 0, \qquad \Pi_3 = 0. \tag{2.2}$$

That is,

$$\Pi_k = \bar{\mathbf{v}} \cdot \mathbf{E}_k + (\boldsymbol{\omega} \times \boldsymbol{\pi}_P) \cdot \mathbf{E}_k, \qquad (k = 1, 2, 3)\,, \tag{2.3}$$

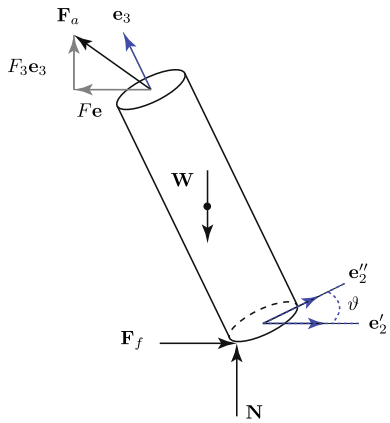

Fig. 2 The forces acting on the cylinder are the weight $\mathbf{W} = -mg\mathbf{E}_3$ acting at its center of mass, the normal force $\mathbf{N} = N\mathbf{E}_3$ and the friction force $\mathbf{F}_f = F_{f_1}\mathbf{E}_1 + F_{f_2}\mathbf{E}_2$ acting at the contact between the cylinder and the ground, and an applied force $\mathbf{F}_a = F_1\mathbf{E}_1 + F_2\mathbf{E}_2 + F_3\mathbf{E}_3$ at mid point of the upper surface of the cylinder

where

$$\boldsymbol{\pi}_P = -\frac{h}{2}\mathbf{e}_3 - r\mathbf{e}_2'', \tag{2.4}$$

and representations for $\mathbf{e}_2''$ and $\boldsymbol{\omega}$ can be found in (A2), (A3), and (A5) in Appendix A. The constraints functions (2.2) can be expressed in their component forms:

$$\begin{aligned}
\Pi_1 &= \dot{x}_1 + f_1 \cos(\psi)\,\dot{\psi} - f_2 \sin(\psi)\,\dot{\vartheta} + r\cos(\psi)\,\dot{\varphi},\\
\Pi_2 &= \dot{x}_2 + f_1 \sin(\psi)\,\dot{\psi} + f_2 \cos(\psi)\,\dot{\vartheta} + r\sin(\psi)\,\dot{\varphi},\\
\Pi_3 &= \dot{x}_3 - f_1\dot{\vartheta},
\end{aligned} \tag{2.5}$$

where

$$\begin{aligned}
f_1 &= r\cos(\vartheta) - \frac{h}{2}\sin(\vartheta),\\
f_2 &= r\sin(\vartheta) + \frac{h}{2}\cos(\vartheta).
\end{aligned} \tag{2.6}$$

As discussed in Appendix B, the system of constraints (2.2) are non-integrable (or non-holonomic). In addition, the constraint $\Pi_3 = 0$ is integrable and implies that $x_3 = r\sin(\vartheta) + \frac{h}{2}\cos(\vartheta)$ modulo a constant.

Referring to Fig. 2, the forces acting on the cylinder are a gravitational force $-mg\mathbf{E}_3$ acting at $\bar{X}$, a normal $N\mathbf{E}_3$ and static friction force $\mathbf{F}_f = F_{f_1}\mathbf{E}_1 + F_{f_2}\mathbf{E}_2$ acting at the instantaneous point of contact P, and an applied force $\mathbf{F}_a$ acting at a point X_a on the upper extremities of the cylinder: $\boldsymbol{\pi}_a = \frac{h}{2}\mathbf{e}_3$. The cylinder is assumed to be axisymmetric with an inertia tensor

$$\mathbf{J} = \lambda_t\,(\mathbf{e}_1 \otimes \mathbf{e}_1 + \mathbf{e}_2 \otimes \mathbf{e}_2) + \lambda_a \mathbf{e}_3 \otimes \mathbf{e}_3, \tag{2.7}$$

where λ_t and λ_a are moments of inertia. The balance laws for the cylinder are

$$\begin{aligned}
&\mathbf{F}_a + \mathbf{F}_f + (N - mg)\,\mathbf{E}_3 = m\dot{\bar{\mathbf{v}}},\\
&\boldsymbol{\pi}_a \times \mathbf{F}_a + \boldsymbol{\pi}_P \times \left(\mathbf{F}_f + N\mathbf{E}_3\right) = \mathbf{J}\dot{\boldsymbol{\omega}} + \boldsymbol{\omega} \times (\mathbf{J}\boldsymbol{\omega}),
\end{aligned} \tag{2.8}$$

where $\boldsymbol{\pi}_a = \frac{h}{2}\mathbf{e}_3$. These balance laws are supplemented by the constraints (2.2) to form a determinate system of equations to compute the motion of the cylinder and the normal and static friction forces.

3 Supporting rectilinear motions of a cylinder

We start by considering the simplest possible locomotion for an inclined cylinder: rectilinear motion of the center of mass at constant speed. The goal of our analysis is to determine the applied force $\mathbf{F}_a$ required to sustain the motion. For the motion of interest, two of the Euler angles are constant and the spin rate $\dot{\varphi}$ is constant:

$$\dot{\psi} = 0, \qquad \dot{\vartheta} = 0, \qquad \dot{\varphi} = \omega_0. \tag{3.1}$$

The constraints (2.2) are satisfied provided

$$\bar{\mathbf{v}} = -r\omega_0\mathbf{e}_1'. \tag{3.2}$$

The balances of linear and angular momenta (2.8) simplify dramatically:

$$\begin{aligned}
&F\mathbf{e} + F_3\mathbf{E}_3 + F_{f_1}\mathbf{E}_1 + F_{f_2}\mathbf{E}_2\\
&\quad + N\mathbf{E}_3 - mg\mathbf{E}_3 = \mathbf{0},\\
&\left(-\frac{h}{2}\mathbf{e}_3 - r\mathbf{e}_2''\right) \times (N\mathbf{E}_3 - F\mathbf{e})\\
&\quad + \frac{h}{2}\mathbf{e}_3 \times (F\mathbf{e} + F_3\mathbf{E}_3) = \mathbf{0},
\end{aligned} \tag{3.3}$$

where the unit vector $\mathbf{e} = \beta_1 \mathbf{e}'_1 + \beta_2 \mathbf{e}'_2$. With the help of equation $(3.3)_1$, we conclude that

$$\begin{aligned} &N + F_3 = mg, \\ &F_{f_1}\mathbf{E}_1 + F_{f_2}\mathbf{E}_2 = -F\mathbf{e}. \end{aligned} \tag{3.4}$$

After expressing the balance of angular momentum $(3.3)_2$ in components with respect to the $\{\mathbf{e}'_1, \mathbf{e}'_2, \mathbf{E}_3\}$ basis, we find that:

$$\begin{aligned} &N\left(\frac{h}{2}\sin(\vartheta) - r\cos(\vartheta)\right) - F_3\frac{h}{2}\sin(\vartheta) \\ &\quad - F\beta_2\left(r\sin(\vartheta) + h\cos(\vartheta)\right) = 0, \\ &F\beta_1\left(r\sin(\vartheta) + h\cos(\vartheta)\right) = 0, \\ &-F\beta_1\left(r\cos(\vartheta) - h\sin(\vartheta)\right) = 0. \end{aligned} \tag{3.5}$$

We conclude from the component forms that $\beta_1 = 0$ and then set $\beta_2 = 1$. That is, the friction force serves solely to balance the horizontal component of the applied force: $\mathbf{F}_f = -F\mathbf{e}'_2$. Using $(3.4)_1$ to eliminate $F_3 = mg - N$, we find that the balance of angular momentum reduces to a single non-trivial equation:

$$\begin{aligned} &N\left(r\cos(\vartheta) - h\sin(\vartheta)\right) + \frac{mgh}{2}\sin(\vartheta) \\ &= -F\left(r\sin(\vartheta) + h\cos(\vartheta)\right). \end{aligned} \tag{3.6}$$

The friction force $\mathbf{F}_f$ is subject to the static friction criterion: $\sqrt{F_{f1}^2 + F_{f2}^2} = |F| \leq \mu_s N$ where μ_s is the coefficient of static friction. In order to establish the range of feasible angles of inclination as a function of the applied force F_3, we examine extreme cases of maximum static friction force $|F| = \mu_s N$:

$$\begin{aligned} &\mu_s N\left(r\sin(\vartheta) + h\cos(\vartheta)\right) \\ &= \left|\frac{mgh}{2}\sin(\vartheta) + N\left(r\cos(\vartheta) - h\sin(\vartheta)\right)\right|. \end{aligned} \tag{3.7}$$

This equality is equivalent to a pair of identities:

$$\begin{aligned} &\frac{mg - F_3}{mg} = \frac{N}{mg} \\ &= \frac{\frac{1}{2}\sin(\vartheta)}{\sin(\vartheta) - \frac{r}{h}\cos(\vartheta) \pm \mu_s\left(\frac{r}{h}\sin(\vartheta) + \cos(\vartheta)\right)}. \end{aligned} \tag{3.8}$$

The condition that $N > 0$ and $F_3 > 0$ are simultaneously satisfied implies that $0 < \frac{N}{mg} < 1$ and also places a restriction on the allowable range of the angle of inclination ϑ:

$$\begin{aligned} &\vartheta \in \left(\max\left(0,\ \tan^{-1}\left(\frac{\frac{r}{h} - \mu_s}{\frac{1}{2} + \frac{r\mu_s}{h}}\right)\right), \frac{\pi}{2}\right) \\ &\text{in the } (+) \text{ case}, \\ &\vartheta \in \left(\max\left(0,\ \cot^{-1}\left(\frac{\frac{1}{2} - \frac{r\mu_s}{h}}{\frac{r}{h} + \mu_s}\right)\right), \frac{\pi}{2}\right) \\ &\text{in the } (-) \text{ case}. \end{aligned} \tag{3.9}$$

For a given inclination of the cylinder (i.e., a given value of ϑ), two limiting friction force distributions with distinct applied forces $\mathbf{F}_a$ are possible. At the transitional case where the horizontal plane is smooth ($\mu_s = 0$), (3.8) simplifies to

$$\begin{aligned} &\frac{mg - F_3}{mg} = \frac{N}{mg} = \frac{\frac{1}{2}\sin(\vartheta)}{\sin(\vartheta) - \frac{r}{h}\cos(\vartheta)}, \\ &\vartheta \in \left(\tan^{-1}\left(\frac{2r}{h}\right), \frac{\pi}{2}\right). \end{aligned} \tag{3.10}$$

To explore possible inclinations of the cylinder, we plot $\frac{mg}{N}$ as a function of the angle of inclination for three limiting cases: $\mathbf{F}_f = -\mu_s N\mathbf{e}'_2$, $\mathbf{F}_f = \mathbf{0}$, and $\mathbf{F}_f = \mu_s N\mathbf{e}'_2$. These cases are defined by $(3.8)_-$, (3.10), and $(3.8)_+$, respectively. The results are shown in Figs. 3, 4 and 5. From these figures we observe that not all possible combinations of F_3 and ϑ are possible because of the limiting value of the static friction force. The results shown in Figs. 4 and 5 demonstrate how the range in feasible values of (ϑ, F_3) depends on the geometry of the cylinder and the static coefficient of friction.

Referring to Fig. 4, we observe that the curves for the case $\mathbf{F}_f = \mu_s N\mathbf{e}'_2$ (i.e., $(3.8)_+$) intersect at a single point that is independent of $\frac{r}{h}$. We can compute the coordinates of this point from (3.8) by combining the $\frac{r}{h}$ terms and setting their coefficient to be zero:

$$\left(\vartheta = \tan^{-1}\left(\frac{1}{\mu_s}\right),\ \frac{N}{mg} = \frac{1}{2\left(1 + \mu_s^2\right)}\right). \tag{3.11}$$

We also note the points where $N = mg$ and $F_3 = 0$ at which the inclined cylinder is in equilibrium under

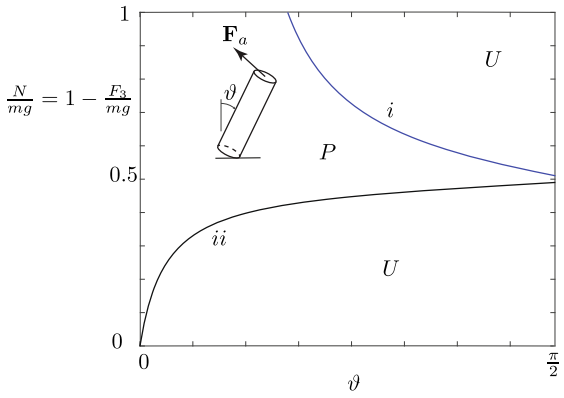

Fig. 3 The space of possible configurations of the inclined rolling cylinder displayed as a function of the angle of inclination ϑ and the dimensionless force $\frac{N}{mg} = 1 - \frac{F_3}{mg}$. The bounding curves correspond to the restriction imposed by the static friction criterion. For the regions labeled P - which is bounded by the curves labelled i and ii and $\vartheta > 0$, the motions of interest are possible. The motions are not possible for pairs (ϑ, N) in the regions labeled U. The bounding curve labelled i is obtained from $(3.8)_-$ and the bounding curve labelled ii is computed from $(3.8)_+$. The results shown in this figure pertain to the case where $\mu_s = 0.2$ and $\frac{r}{h} = 0.1$

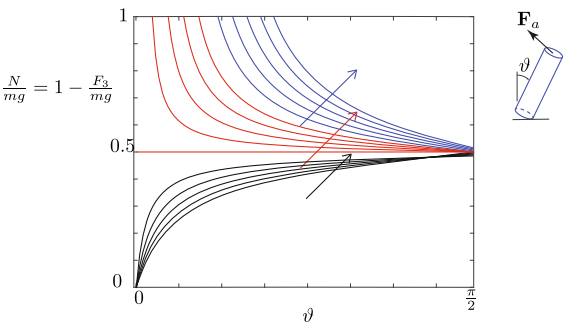

Fig. 4 The dimensionless force $1 - \frac{F_3}{mg}$ as a function of the angle of inclination ϑ. The black curves are obtained from $(3.8)_+$, the red curves from (3.10) (i.e., $(3.8)_{\mu_s=0}$), and the blue curves are obtained from $(3.8)_-$ for $\mu_s = 0.2$ and various values of $\frac{r}{h}$. The arrows point in direction of increasing $\frac{r}{h}$ from 0 to 0.15. When $\frac{r}{h} = 0$, the cylinder is a slender rod of length h while at the other extreme when $\frac{r}{h} = \infty$ the rigid body is circular disk of radius r

the action of its weight, normal and friction forces, and an applied force that counterbalances the friction force: $\mathbf{F}_a = -\mathbf{F}_f$. As evidenced by the results shown in Fig. 5, the larger the value of μ_s then the larger the range of angles of inclination ϑ for a given F_3.

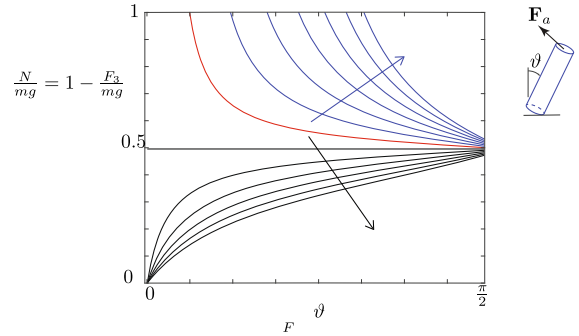

Fig. 5 The dimensionless force $1 - \frac{F_3}{mg}$ as a function of the angle of inclination ϑ. The black curves are obtained from $(3.8)_+$, the red curves from (3.10) (i.e., $(3.8)_{\mu_s=0}$), and the blue curves are obtained from $(3.8)_-$ for $\frac{r}{h} = 0.1$ and various values of $\mu_s = 0, 0.1, 0.2, 0.3, 0.4, 0.5, 0.6$. The arrows point in direction of increasing μ_s. The results for $\mu_s = 0$ coincide with the red curve

3.1 The smallest force

The results so far show that the same angle of inclination ϑ can be sustained by multiple values of the applied force $\mathbf{F}_a$. The multiplicity is made possible by the nature of the static friction force. It is of interest to see if there is a minimum force. More precisely, for given values of μ_s and $\frac{r}{h}$, what is the minimum force $\|\mathbf{F}_a\|$ required to maintain a given angle of inclination ϑ?

To answer the question, we return to (3.6) and eliminate N using the identity $N = mg - F_3$. After some rearranging, we find an expression for the dimensionless horizontal component of $\mathbf{F}_a$:

$$\frac{F}{mg} = \alpha_1 \left(\frac{F_3}{mg}\right) + \alpha_2, \tag{3.12}$$

where

$$\alpha_1 = \frac{\frac{r}{h}\cos(\vartheta) - \sin(\vartheta)}{\frac{r}{h}\sin(\vartheta) + \cos(\vartheta)},$$
$$\alpha_2 = -\frac{\frac{r}{h}\cos(\vartheta) - \frac{1}{2}\sin(\vartheta)}{\frac{r}{h}\sin(\vartheta) + \cos(\vartheta)}. \tag{3.13}$$

If we seek to compute the minimum applied force for a given ϑ, then a geometric argument applied to the linear relation (3.12) in the $F_3 - F$ space, shows that the point on the line (3.12) closest to the origin is found by the intersection of this line with the perpendicular

intercept:

$$\frac{F}{mg} = -\frac{1}{\alpha_1}\left(\frac{F_3}{mg}\right). \tag{3.14}$$

That is,

$$\left(\frac{F_3}{mg} = -\frac{\alpha_1\alpha_2}{1+\alpha_1^2}, \quad \frac{F}{mg} = \frac{\alpha_2}{1+\alpha_1^2}\right). \tag{3.15}$$

Thus, the minimum magnitude of the applied force for given values of $\frac{r}{h}$ and ϑ is

$$\|\mathbf{F}_a\| = \frac{mg|\alpha_2|}{\sqrt{1+\alpha_1^2}} = \frac{mg}{\sqrt{1+\left(\frac{r}{h}\right)^2}}\left|\frac{r}{h}\cos(\vartheta) - \frac{1}{2}\sin(\vartheta)\right|. \tag{3.16}$$

The solution (3.15) to the minimum force problem is valid provided the static friction criterion, $|F| \leq \mu_s N = \mu_s(mg - F_3)$, is satisfied:

$$|\alpha_2| \leq \mu_s\left(\alpha_1^2 + \alpha_1\alpha_2 + 1\right). \tag{3.17}$$

A representative case, labeled i, where (3.14) is used to compute the minimum applied force is shown in Fig. 6.

If (3.15) does not satisfy (3.17), then the minimizing solution must be found by seeking the point on the line (3.12) that is closest to the origin that satisfies $|F| \leq \mu_s N = \mu_s(mg - F_3)$. A representative case where (3.15) does not yield a minimal applied force that satisfies the static friction condition (3.17), is shown in Fig. 6 where it is labeled ii. Consider the case where the point which minimizes the applied force $\mathbf{F}_a$ lies at the intersection of the line (3.12) with $\mu_s N = \mu_s(mg - F_3) = F$ or $\mu_s N = \mu_s(mg - F_3) = -F$, depending on whichever minimizes that $\mathbf{F}_a$. The intersection points in the positive and negative cases are, respectively,

$$\begin{aligned}&\left(\frac{F_3}{mg} = \frac{\mu_s - \alpha_2}{\mu_s + \alpha_1}, \quad \frac{F}{mg} = \mu_s\frac{\alpha_1 + \alpha_2}{\mu_s + \alpha_1}\right),\\ &\left(\frac{F_3}{mg} = \frac{\mu_s + \alpha_2}{\mu_s - \alpha_1}, \quad \frac{F}{mg} = \mu_s\frac{\alpha_1 + \alpha_2}{\mu_s - \alpha_1}\right).\end{aligned} \tag{3.18}$$

The third and penultimate case we need to consider arises when the line (3.12) intersects the vertical axis

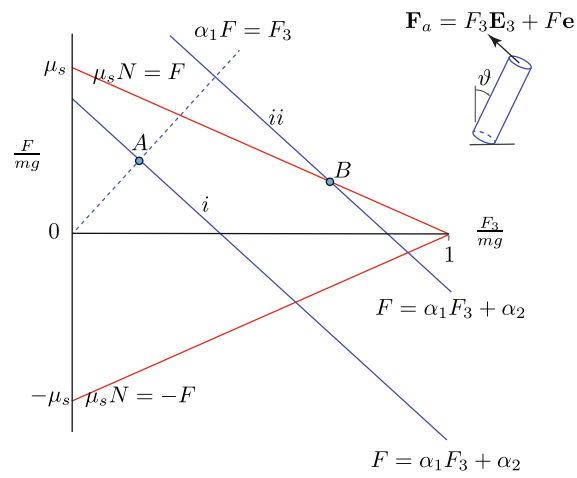

Fig. 6 The space $\frac{F_3}{mg} - \frac{F}{mg}$ showing the admissible region defined by the static friction criterion $|F| \leq \mu_s N$ and two examples of the linear relation (3.12). For the example labelled i, the point corresponding to the minimum force $|\mathbf{F}_a|$ is labelled A and can be computed using (3.15). For the example labelled ii, the minimum force $|\mathbf{F}_a|$ computed using (3.15) does not satisfy the static friction criterion and the minimum force (labelled B) is computed using (3.18). The angle ϑ and parameters $\frac{r}{h}$ and μ_s are all assumed to be constant

$\frac{F_3}{mg} = 0$ and the restriction $F_3 \geq 0$ is imposed. In this case, the minimizing value of $||\mathbf{F}_a|| = mg\,|\alpha_2|$. The corresponding values of the components of $\mathbf{F}_a$ are

$$\left(\frac{F_3}{mg} = 0, \quad \frac{F}{mg} = \alpha_2\right). \tag{3.19}$$

The fourth case arises when the cylinder is vertical ($\vartheta = 0$) or completely horizontal. In these cases, the normal force is balanced by gravity, the friction force vanishes, and the minimum $\mathbf{F}_a = \mathbf{0}$. In summary, four sets of values of $(F_3/mg, F/mg)$ are used to compute minimum values of $\|\mathbf{F}_a\|$ for $\vartheta \in [0, 90°]$.

As shown in Fig. 7, we consider a fixed value of $\frac{r}{h} = 0.1$ and a fixed $\mu_s = 0.2$ and vary $\vartheta \in (0, 90°)$. With the help of (3.17) and (3.18), the locus of points $(F_3/mg, F/mg)$ corresponding to minimum values of $\|\mathbf{F}_a\|$ are computed. Referring to the figure, the points B and C correspond to the intersection points of the families of lines (3.12) and (3.14), respectively, for a given $\frac{r}{h}$ value. The coordinates of these points are

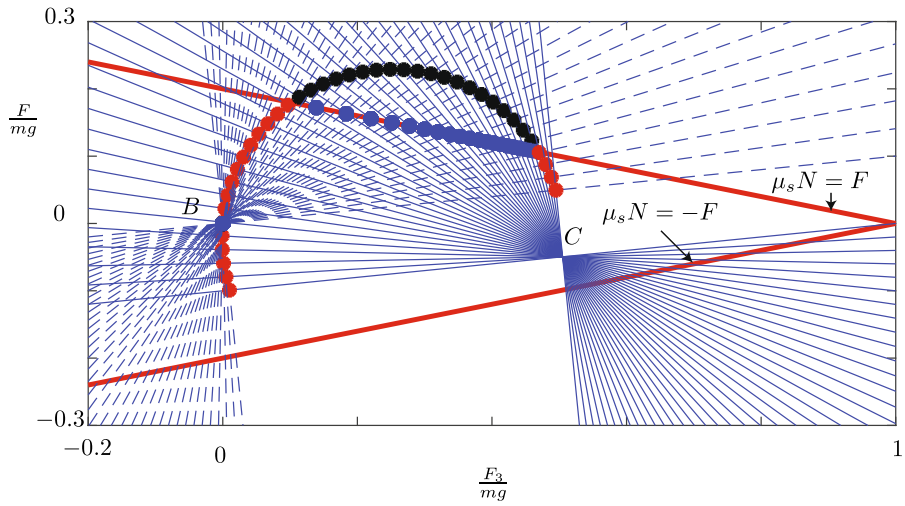

Fig. 7 The components of the minimum force $\mathbf{F}_a$ in the $\frac{F_3}{mg} - \frac{F}{mg}$ plane trace a circle with diameter BC given by (3.20) for $\vartheta \in (0, 90°)$. The points belonging to the aforementioned circle for which (3.17) is satisfied are drawn in red, otherwise, they are drawn in black. In the latter case, the force minimizing points that satisfy the static friction criterion are drawn in blue, and belong either to the lines $\mu_s N = \pm F$ or $F_3 = 0$

$$B = \left(\frac{F_3}{mg} = 0, \quad \frac{F}{mg} = 0\right),$$
$$C = \left(\frac{F_3}{mg} = \frac{\frac{1}{2} + \left(\frac{r}{h}\right)^2}{1 + \left(\frac{r}{h}\right)^2}, \quad \frac{F}{mg} = \frac{-\frac{1}{2}\frac{r}{h}}{1 + \left(\frac{r}{h}\right)^2}\right). \tag{3.20}$$

Since the lines (3.12) and (3.14) always pass through the points B and C respectively, and are perpendicular. Thus, the locus of the intersection point of these lines is a circle of diameter BC.

One might expect that the minimum applied force is a vertical force $\mathbf{F}_a = F_3\mathbf{E}_3$ as the friction force supplied by the ground for equilibrium would necessarily vanish. However, apart from the case $\vartheta = \tan^{-1}\left(\frac{2r}{h}\right)$, this is not the case. To elaborate, for a given cylinder and contacting plane, the components of the minimum applied force as a function of ϑ are shown in Fig. 8. The point labelled D corresponds to the absolute minimum applied force which is $\|\mathbf{F}_a\| = 0$ which arises when the angle of inclination $\vartheta = \tan^{-1}\left(\frac{2r}{h}\right)$. The cylinder self balances at this angle of inclination and the static friction force vanishes. The graphs of $\|\mathbf{F}_a\|(\vartheta)$, $F(\vartheta)$, and $F_3(\vartheta)$ are discontinuous at $\vartheta = 0, 90°$ as the minimum applied force $\mathbf{F}_a = \mathbf{0}$ at these points. The two points are labelled E in Fig. 8 and signify discontinuities in the graphs of $F(\vartheta)$ and $F_3(\vartheta)$ as $\vartheta \searrow 0$ and $\vartheta \nearrow \frac{\pi}{2}$.

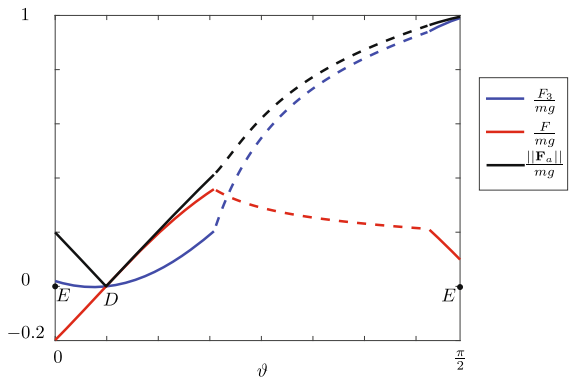

Fig. 8 The minimum force satisfying the static friction criterion vs. ϑ for $\mu_s = 0.2$ and $\frac{r}{h} = 0.1$. The continuous portion of the curve corresponds to solutions of (3.15) satisfying (3.17). In the regions where (3.17) is not satisfied, the curve is dashed with relevant values given either by (3.18) or (3.19). The points labeled E correspond to the minimum values of $\mathbf{F}_a = \mathbf{0}$ when $\vartheta = 0, 90°$

4 Holonomies of a rolling cylinder

Consider a cylinder rolling on a horizontal surface while its center of mass traces out a closed path. After the center of mass has returned to its original location, we will typically find that the orientation of the cylinder has changed. The change in orientation is known as a holonomy. Holonomies in rigid body dynamics can be attributed to the non-holonomic constraints on the motion of the body. The phenomenon in rolling spheres with application to spherical robots has been discussed in [7–9] and discussions of holonomy in parallel parking can be found in [15,16].

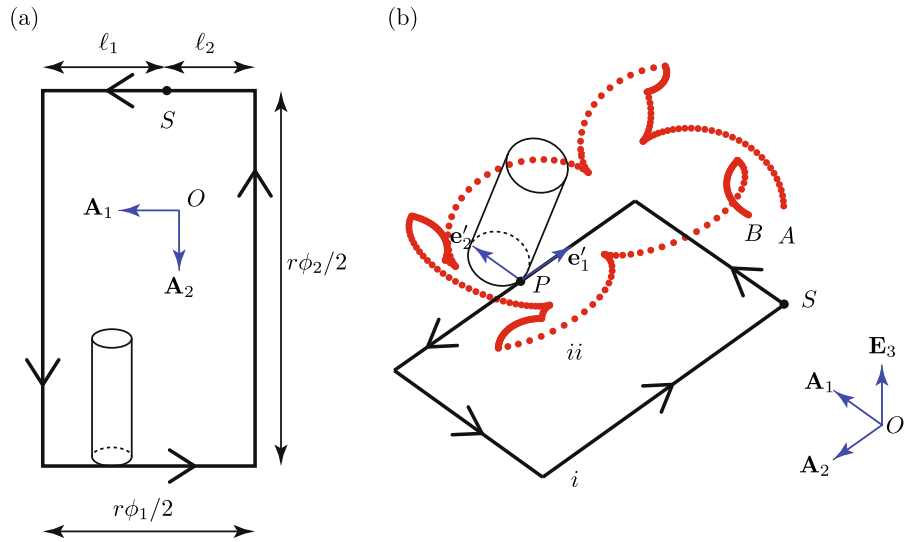

Fig. 9 **a** The rectangular path traced by the instantaneous point of contact P between the cylinder and the horizontal plane. The cylinder starts the circumnavigation at the point labeled S. The location of S is defined by the parameter $s \in [0, 1]$: $\ell_1 = \frac{r(1-s)\phi_1}{2}$ and $\ell_2 = \frac{rs\phi_1}{2}$. The rectangle has sides of length $\frac{r\phi_1}{2}$ and $\frac{r\phi_2}{2}$ and produces a holonomy of $\phi_1 + \phi_2$ in the rolling inclined cylinder. **b** Time traces of the point P and of a material point X on the rim of the cylinder as P traces the rectangular path. The traces are labelled i and ii respectively. While the center of mass returns to its original location S, X has relocated from A to B. The example shown is classified as Case I

Recall that we are using a set of 3-1-3 Euler angles to parameterize the rotation of the cylinder. The angles $\psi \in [0, 2\pi]$ and $\vartheta = [0, \pi]$ can each be individually altered without changing the other angles or the location of the instantaneous point of contact P. As a result, and in contrast to our earlier work on the holonomy of rolling spheres [9], we restrict attention to motions of the cylinder that produce changes in φ. The two motions of interest are those where the instantaneous point of contact traces out a rectangular path and a circular path. We now establish closed form expressions for the change in orientation (holonomy) for both types of path.

4.1 Holonomy of a rolling cylinder tracing a rectangular path

If we imagine an inclined rolling cylinder tracing a closed rectangular path starting at a point S, then the change in the angle φ when the center of mass has returned to its original location will typically be nontrivial. The change in the angle φ is an example of a holonomy. As we shall explain, the change in the angle is not only a function of the lengths of the sides of the rectangles, whether or not the path is traversed in a counterclockwise or clockwise manner, the angle ϑ of inclination of the rectangle, and whether the unit vector $\mathbf{e}'_2$ points inward or outward to the path. We refer to these two instances as Case I and Case II, respectively. The holonomy will be shown to be independent of the choice of starting point S.

To proceed with our analysis, we consider Case I. Now consider a rectangle with side lengths $\frac{r\phi_1}{2}$ and $\frac{r\phi_2}{2}$ as depicted in Fig. 9. Without loss in generality, the starting point S is specified by the parameter $s \in [0, 1]$. The Cartesian basis vectors $\mathbf{A}_1$ and $\mathbf{A}_2$ are each parallel to two sides of the rectangle. Tracing a rectangular path in a counterclockwise manner using a rolling cylinder is achieved using two types of motion: rotations about $\mathbf{e}_3$ and rotations about $\mathbf{E}_3$. For the first of these, $\boldsymbol{\omega} = \dot{\varphi}\mathbf{e}_3$, and the constraints $\mathbf{v}_P = \mathbf{0}$ imply that

$$\bar{\mathbf{v}} = -r\dot{\varphi}\mathbf{e}'_1. \tag{4.1}$$

That is the cylinder's center of mass moves in a straight line. As $\dot{\varphi}_1 > 0$, this implies that $\mathbf{e}'_1$ is antiparallel to the direction of motion and $\mathbf{e}'_2$ is one of the two outward normals to the path. For motions where $\boldsymbol{\omega} = \dot{\psi}\mathbf{E}_3$, the

constraints $\mathbf{v}_P = \mathbf{0}$ implies that

$$\bar{\mathbf{v}} = -\dot{\psi} f_1 \mathbf{e}_1'. \tag{4.2}$$

These motions enable the cylinder to turn the corners of the rectangle. For the rectangular path shown in Fig. 9, either $\mathbf{e}_1' = \pm\mathbf{A}_1$ or $\mathbf{e}_1' = \pm\mathbf{A}_2$.

Tracing the rectangle depicted in Fig. 9(a) in a counterclockwise direction requires the cylinder to undergo a sequence of nine rotations. The combined rotation, which is also the change in orientation of the cylinder, is $\mathbf{S}$ where

$$\begin{aligned}\mathbf{S} &= \hat{\mathbf{S}}_I\left(\vartheta, \phi_1, \phi_2, s, r, h, \psi_0, \circlearrowleft\right)\\ &= \mathbf{A}\left(\frac{s\phi_1}{2}, {}_0\mathbf{e}_3\right)\mathbf{A}\left(\frac{\pi}{2}, \mathbf{E}_3\right)\mathbf{A}\left(\frac{\phi_2}{2}, {}_3\mathbf{e}_3\right)\\ &\quad \mathbf{A}\left(\frac{\pi}{2}, \mathbf{E}_3\right)\mathbf{A}\left(\frac{\phi_1}{2}, {}_2\mathbf{e}_3\right)\\ &\quad \times \mathbf{A}\left(\frac{\pi}{2}, \mathbf{E}_3\right)\mathbf{A}\left(\frac{\phi_2}{2}, {}_1\mathbf{e}_3\right)\mathbf{A}\left(\frac{\pi}{2}, \mathbf{E}_3\right)\\ &\quad \mathbf{A}\left(\frac{(1-s)\,\phi_1}{2}, {}_0\mathbf{e}_3\right)\end{aligned} \tag{4.3}$$

where $\mathbf{A}(\xi, \mathbf{r})$ denotes a rotation about an axis $\mathbf{r}$ through a counterclockwise angle of rotation ξ,

$$\begin{aligned}{}_i\mathbf{e}_3 &= \mathbf{A}\left(\frac{i\pi}{2}, \mathbf{E}_3\right){}_0\mathbf{e}_3, \qquad (i = 1, 2, 3),\\ {}_0\mathbf{e}_3 &= \sin(\psi_0)\sin(\vartheta)\,\mathbf{E}_1 - \cos(\psi_0)\sin(\vartheta)\,\mathbf{E}_2\\ &\quad + \cos(\vartheta)\,\mathbf{E}_3.\end{aligned} \tag{4.4}$$

The parameter $\circlearrowleft, \circlearrowright$ in $\hat{\mathbf{S}}$ is used to distinguish counterclockwise and clockwise directions, respectively, of circumnavigating the rectangular path. Computing the products of the rotations in (4.3), we conclude that

$$\hat{\mathbf{S}}_I\left(\vartheta, \phi_1, \phi_2, s, r, h, \psi_0, \circlearrowleft\right) = \mathbf{A}\left(\phi_1 + \phi_2, {}_0\mathbf{e}_3\right). \tag{4.5}$$

That is, the holonomy is

$$\Delta\varphi = \phi_1 + \phi_2. \tag{4.6}$$

We observe that $\mathbf{A}(2n\pi, {}_0\mathbf{e}_3) = \mathbf{I}$, where $\mathbf{I}$ is the identity tensor. Thus, we can increase the lengths of the sides of the rectangle by integer multiples of 2π without changing the holonomy $\Delta\varphi$. If we were to traverse the rectangle in a clockwise manner, then the sign of the holonomy reverses:

$$\hat{\mathbf{S}}_I\left(\vartheta, \phi_1, \phi_2, s, r, h, \psi_0, \circlearrowright\right) = \mathbf{A}\left(-\phi_1 - \phi_2, {}_0\mathbf{e}_3\right). \tag{4.7}$$

That is, $\Delta\varphi = -\phi_1 - \phi_2$.

For Case II, the expression (4.1) for $\bar{\mathbf{v}}$ holds, however $\dot{\varphi} < 0$. Assuming the path is circumnavigated in a counterclockwise manner, the unit vector $\mathbf{e}_2'$ now points inwards. The expression for $\hat{\mathbf{S}}_{II}$ is readily established by changing the signs of ϕ_1 and ϕ_2 in (4.3). The resulting holonomies are

$$\begin{aligned}\hat{\mathbf{S}}_{II}\left(\vartheta, \phi_1, \phi_2, s, r, h, \psi_0, \circlearrowleft\right) &= \mathbf{A}\left(-\phi_1 - \phi_2, {}_0\mathbf{e}_3\right),\\ \hat{\mathbf{S}}_{II}\left(\vartheta, \phi_1, \phi_2, s, r, h, \psi_0, \circlearrowright\right) &= \mathbf{A}\left(\phi_1 + \phi_2, {}_0\mathbf{e}_3\right).\end{aligned} \tag{4.8}$$

As the expressions for the angle and axes of the holonomies are independent of s, we conclude that the holonomies (4.6), (4.7), and (4.8) are independent of the starting point S. Representative examples of Case I and Case II are shown in Fig. 10.

We can also verify (4.6) and (4.8) using a quaternion representation of a rotation and the Rodrigues formula for compound rotations.[2] Restricting attention to Case I, repeated application of the Rodrigues formula to (4.3) shows that the unit quaternion associated with the rotation $\hat{\mathbf{S}}_I\left(\vartheta, \phi_1, \phi_2, s, r, h, \psi_0, \circlearrowleft\right)$ has the representation

$$\begin{aligned}q_0 &= \cos\left(\frac{\gamma}{2}\right) = \cos\left(\pi + \frac{\phi_1}{2} + \frac{\phi_2}{2}\right),\\ \mathbf{q} &= \sin\left(\frac{\gamma}{2}\right)\mathbf{r} = \sin\left(\pi + \frac{\phi_1}{2} + \frac{\phi_2}{2}\right){}_0\mathbf{e}_3,\end{aligned} \tag{4.9}$$

where γ is the angle of rotation and $\mathbf{r}$ is the axis of rotation: a result that is in agreement with (4.6). The analysis for Case II is similar and in the interests of brevity is not presented here.

[2] Consider a pair of rotations $\mathbf{A} = \tilde{\mathbf{A}}(a_0, \mathbf{a})$ and $\mathbf{B} = \tilde{B}(b_0, \mathbf{b})$ parameterized by unit quaternions $(a_0, \mathbf{a})$ and $(b_0, \mathbf{b})$, respectively. Then, the compound rotation $\mathbf{C} = \mathbf{BA}$ is parameterized by the unit quaternion.

$$\begin{aligned}c_0 &= a_0 b_0 - \mathbf{a}\cdot\mathbf{b},\\ \mathbf{c} &= a_0\mathbf{b} + b_0\mathbf{a} + \mathbf{b}\times\mathbf{a}.\end{aligned}$$

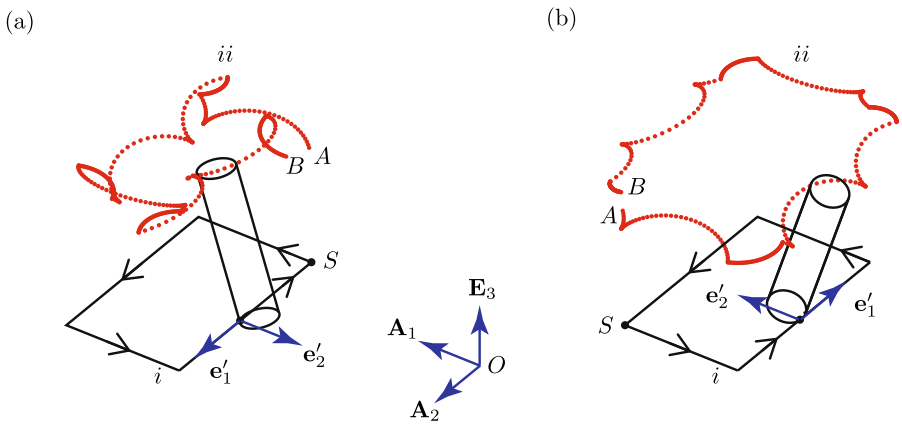

Fig. 10 Motions of a cylinder where the center of mass traces a rectangular path in a counterclockwise manner and produces a holonomy: **a** Case I where $\Delta\varphi = 36.3901^o$ and **b** Case II where $\Delta\varphi = -36.3901^o$. For the results shown in this figure, $h = 8.3333r$, $\phi_1 = \frac{13\pi}{3}$, $\phi_2 = \frac{29\pi}{4}$, $\vartheta = \frac{\pi}{10}$, and $s = 0$

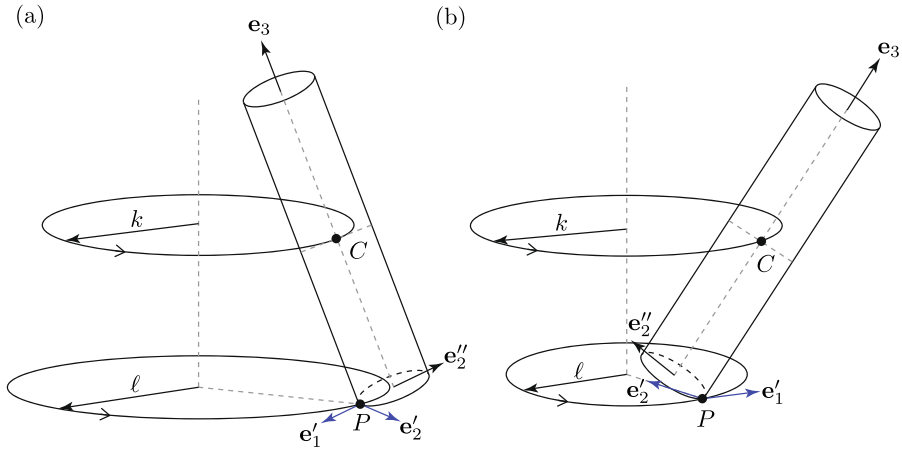

Fig. 11 Motions of a cylinder where the center of mass C traces a circular path of radius k and the instantaneous point of contact P traces a circular path of radius ℓ. Both paths are traced in a counterclockwise manner. **a** Case I where $\mathbf{e}_2'$ points radially outward and **b** Case II where $\mathbf{e}_2'$ points radially inward

4.2 Holonomy of a rolling cylinder tracing a circle

We now turn to the case where the center of mass of the cylinder traces a circular path. We are able to establish a simple expression (4.16) for the radius ℓ of the path of the instantaneous point of contact P to establish any desired relative change in the Euler angle φ of the cylinder. As with the case of a rectangular path and as illustrated in Fig. 11, there are two cases to consider: Case I where $\mathbf{e}_2'$ points radially outward and Case II where $\mathbf{e}_2'$ points radially inwards.

For the motion of interest, ϑ is constant, $\boldsymbol{\omega} = \dot{\psi}_0\mathbf{E}_3 + \dot{\varphi}_0\mathbf{e}_3$, and $\dot{\psi}_0$ and $\dot{\varphi}_0$ are constant. The constraints (2.2) imply that

$$\bar{\mathbf{v}} = v_0\mathbf{e}_1' \tag{4.10}$$

where

$$\mathbf{e}_1' = \cos(\psi)\,\mathbf{E}_1 + \sin(\psi)\,\mathbf{E}_2, \quad v_0 = -f_1\dot{\psi}_0 - r\dot{\varphi}_0. \tag{4.11}$$

For a motion to be possible with $\dot{\psi}_0 \neq 0$ and $\dot{\varphi} \neq 0$, the center of mass traces a circle in a counterclockwise manner: that is, the orbital speed $\dot{\psi}_0 > 0$. If we let k be the radius of the circular path traced by the center of mass, then

$$\begin{cases} \bar{\mathbf{r}} = k\mathbf{e}_2', \quad \bar{\mathbf{v}} = -k\dot{\psi}_0\mathbf{e}_1' & \text{for Case I,} \\ \bar{\mathbf{r}} = -k\mathbf{e}_2', \quad \bar{\mathbf{v}} = k\dot{\psi}_0\mathbf{e}_1' & \text{for Case II.} \end{cases} \tag{4.12}$$

Combining the previous results, we obtain

$$\begin{cases} \left(\frac{h}{2}\sin(\vartheta) - r\cos(\vartheta)\right)\dot{\psi}_0 - r\dot{\varphi}_0 = -k\dot{\psi}_0 & \text{for Case I,} \\ \left(\frac{h}{2}\sin(\vartheta) - r\cos(\vartheta)\right)\dot{\psi}_0 - r\dot{\varphi}_0 = k\dot{\psi}_0 & \text{for Case II.} \end{cases} \tag{4.13}$$

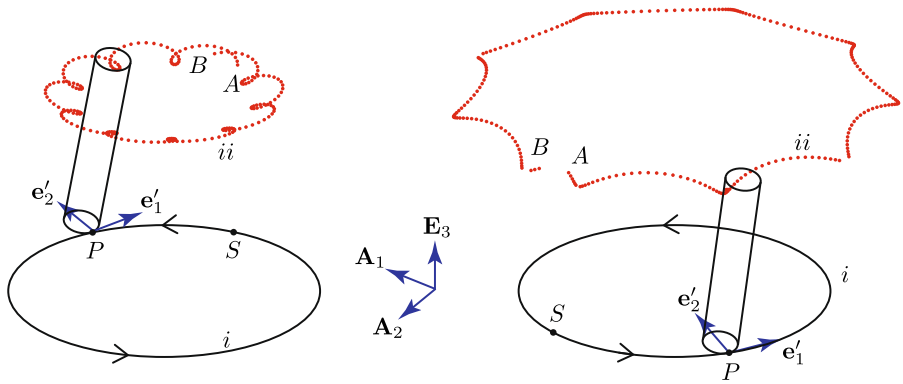

Fig. 12 Time traces of the point P and of a material point X on the rim of the cylinder as P traces the circular path. The traces are labelled i and ii respectively. While the center of mass returns to its original location S, X has relocated from A to B. The radius of the path traced by P is ℓ (cf. (4.14) and (4.15)). For the results shown in these images, $\ell = 9.44233r$, $\vartheta = \frac{\pi}{10}$, and $h = 13.3333r$: **a** Case I where $\bar{\mathbf{r}} = 8.33r\mathbf{e}_2'$ and $\Delta\varphi = 59.3283^o$ and **b** Case II where $\bar{\mathbf{r}} = -10.5515r\mathbf{e}_2'$ and $\Delta\varphi = -59.3283^o$

That is,

$$\begin{cases} k = -\frac{h}{2}\sin(\vartheta) + r\cos(\vartheta) + \frac{r\dot{\varphi}_0}{\dot{\psi}_0} & \text{for Case I,} \\ k = \frac{h}{2}\sin(\vartheta) - r\cos(\vartheta) - \frac{r\dot{\varphi}_0}{\dot{\psi}_0} & \text{for Case II.} \end{cases} \tag{4.14}$$

We observe from (4.12) that if $k = 0$, then the center of mass is stationary. In this case (2.2) implies that $\boldsymbol{\omega} \parallel \boldsymbol{\pi}_P$.[3] If the center of mass traces a circle of radius k in a counterclockwise direction while ϑ is constant, then as $\boldsymbol{\pi}_P \cdot \mathbf{e}_1' = 0$ and $\boldsymbol{\pi}_P \cdot \mathbf{e}_2' = \frac{h}{2}\sin(\vartheta) - r\cos(\vartheta)$, we find that the instantaneous point of contact P traces a circle of radius ℓ such that

$$\begin{cases} \ell - k = \frac{h}{2}\sin(\vartheta) - r\cos(\vartheta) & \text{for Case I,} \\ \ell - k = r\cos(\vartheta) - \frac{h}{2}\sin(\vartheta) & \text{for Case II.} \end{cases} \tag{4.15}$$

To trace a complete circle, we require $\Delta\psi = 2\pi$. We conclude that

$$\begin{cases} \Delta\varphi = \frac{2\pi\ell}{r} & \text{for Case I,} \\ \Delta\varphi = -\frac{2\pi\ell}{r} & \text{for Case II.} \end{cases} \tag{4.16}$$

Thus, we can adjust the radius ℓ of the circular path traced by P to obtain any desired rotation $\Delta\varphi$. Representative examples for the two cases are shown in Fig. 12. If the circular path is traversed in a clockwise manner, then there will be sign changes to the results for $\Delta\varphi$ in (4.16).

[3] The representation $(A5)_2$ can be used to show that $r\dot{\varphi} + f_1\dot{\psi} = 0$ when $\boldsymbol{\omega} \parallel \boldsymbol{\pi}_P$ - a result that is (as expected) consistent with $(4.14)_{k=0}$.

5 Kinematics of a pair of contacting cylinders

Referring to Fig. 1, consider a pair of cylinders each of which is in motion with a single point of instantaneous contact with a horizontal surface. The sides of the cylinders touch each other at a single point and the top of each cylinder is supported by applied forces and moments. The system of two rigid bodies has a total of eight possible permutations of slipping and rolling contacts at the three contact points. For the present purposes, we are interested in examining the set of constraints where one cylinder is spun about its axis while both cylinders are constrained so that their points of contact trace straight parallel lines on the ground.

As shown in Figs. 1 and 13, we identify the individual cylinders using the indices I, 1 and II, 2, respectively. The position vector $\bar{\mathbf{x}}_{I,II}$ of the center of mass $\bar{X}_{I,II}$ of the respective cylinders are parameterised by Cartesian coordinates:

$$\begin{aligned} \bar{\mathbf{x}}_I &= x_{I_1}\mathbf{E}_1 + x_{I_2}\mathbf{E}_2 + x_{I_3}\mathbf{E}_3, \\ \bar{\mathbf{x}}_{II} &= x_{II_1}\mathbf{E}_1 + x_{II_2}\mathbf{E}_2 + x_{II_3}\mathbf{E}_3. \end{aligned} \tag{5.1}$$

Following works on the dynamics of rolling disks and cylinders (cf. [5,17]), it is convenient to use a pair of sets of 3-1-3 Euler angles to parameterize the rotation

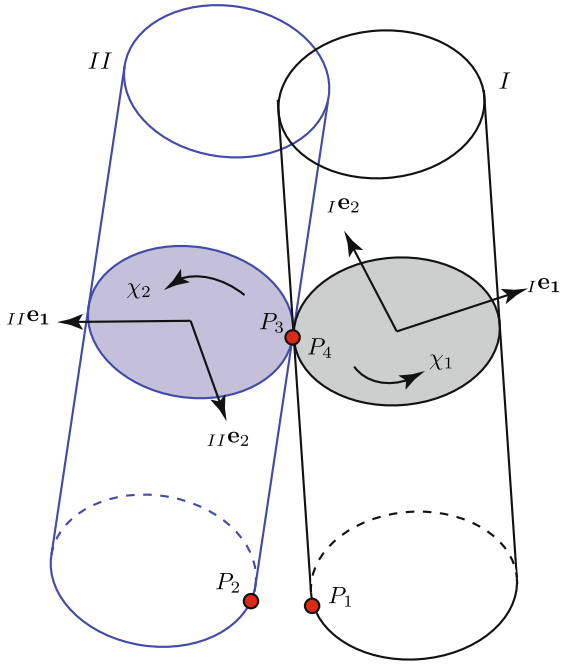

Fig. 13 The instantaneous contact points for the pair of cylinders. The points P_1 and P_2 are the instantaneous points of contact of cylinders I and II, respectively with the horizontal plane and the points P_3 and P_4 are the instantaneous points of mutual contact

of the cylinders.[4] Thus, the rotation tensor $\mathbf{Q}$ and associated angular velocity vectors $\boldsymbol{\omega}$ of the rigid bodies have the following representations:

$$\begin{aligned}
&\mathbf{Q}_I = \mathbf{Q}_I\left(\psi_1, \vartheta_1, \varphi_1\right),\\
&\boldsymbol{\omega}_I = \dot{\psi}_1\,\mathbf{E}_3 + \dot{\vartheta}_1\,{}_I\mathbf{e}_1'' + \dot{\varphi}_1\,{}_I\mathbf{e}_3,\\
&\mathbf{Q}_{II} = \mathbf{Q}_{II}\left(\psi_2, \vartheta_2, \varphi_2\right),\\
&\boldsymbol{\omega}_{II} = \dot{\psi}_2\,\mathbf{E}_3 + \dot{\vartheta}_2\,{}_{II}\mathbf{e}_1'' + \dot{\varphi}_2\,{}_{II}\mathbf{e}_3.
\end{aligned} \tag{5.2}$$

The bases $\left\{\mathbf{E}_3, {}_I\mathbf{e}_1'', {}_I\mathbf{e}_3\right\}$ and $\left\{\mathbf{E}_3, {}_{II}\mathbf{e}_1'', {}_{II}\mathbf{e}_3\right\}$ are the Euler bases associated with the respective sets of Euler angles.

5.1 Formulating the contact constraints

The constraints that cylinder I of height h_1 and radius r_1 rolls without slipping on the horizontal surface can be represented as:

$$\mathbf{v}_1 = \bar{\mathbf{v}}_I + \boldsymbol{\omega}_I \times \boldsymbol{\pi}_{P_1} = \mathbf{0}. \tag{5.3}$$

The position of the instantaneous point of contact P_1 relative to the center of mass has the following representation:

$$\boldsymbol{\pi}_{P_1} = -\frac{h_1}{2}\,{}_I\mathbf{e}_3 - r_1\,{}_I\mathbf{e}_2''. \tag{5.4}$$

In an identical manner, the constraints that cylinder II of height h_2 and radius r_2 rolls without slipping on the horizontal surface have several representations:

$$\mathbf{v}_2 = \bar{\mathbf{v}}_{II} + \boldsymbol{\omega}_{II} \times \boldsymbol{\pi}_{P_2} = \mathbf{0}, \tag{5.5}$$

where

$$\boldsymbol{\pi}_{P_2} = -\frac{h_2}{2}\,{}_{II}\mathbf{e}_3 - r_2\,{}_{II}\mathbf{e}_2''. \tag{5.6}$$

The instantaneous points of contact between the cylinders are denoted by P_3 and P_4. The vectors $\boldsymbol{\pi}_{P_3}$ and $\boldsymbol{\pi}_{P_4}$ are the position vectors of the instantaneous points of contact P_3 and P_4 relative to the centers of mass of the respective cylinders:

$$\begin{aligned}
\mathbf{x}_3 &= \bar{\mathbf{x}}_I + \boldsymbol{\pi}_{P_3},\\
\mathbf{x}_4 &= \bar{\mathbf{x}}_{II} + \boldsymbol{\pi}_{P_4}.
\end{aligned} \tag{5.7}$$

The tangent planes to both cylinders at P_3 and P_4 are identical and spanned by the basis $\{{}_I\mathbf{e}_3,\ {}_{II}\mathbf{e}_3\}$. A unit normal $\mathbf{n}$ can also be defined such that

$$\left\{{}_I\mathbf{e}_3,\ {}_{II}\mathbf{e}_3,\ \mathbf{n} = \frac{{}_I\mathbf{e}_3 \times {}_{II}\mathbf{e}_3}{||{}_I\mathbf{e}_3 \times {}_{II}\mathbf{e}_3||}\right\} \tag{5.8}$$

is a basis for $\mathbb{E}^3$.

The rolling contact between the two cylinders can be described by the vector equation:

$$\mathbf{v}_3 = \mathbf{v}_4, \tag{5.9}$$

where

$$\begin{aligned}
\mathbf{v}_3 &= \bar{\mathbf{v}}_I + \boldsymbol{\omega}_I \times \boldsymbol{\pi}_{P_3}, \qquad \mathbf{x}_3 = \bar{\mathbf{x}}_I + \boldsymbol{\pi}_{P_3},\\
\mathbf{v}_4 &= \bar{\mathbf{v}}_{II} + \boldsymbol{\omega}_{II} \times \boldsymbol{\pi}_{P_4}, \qquad \mathbf{x}_4 = \bar{\mathbf{x}}_{II} + \boldsymbol{\pi}_{P_4}.
\end{aligned} \tag{5.10}$$

[4] Additional background on the 3-1-3 set of Euler angles can be found in Appendix A and in [10, Chapter 6, Section 8.2].

In these representations, $\boldsymbol{\pi}_{P_3}$ and $\boldsymbol{\pi}_{P_4}$ are the position vectors of the instantaneous points of contact P_3 and P_4 relative to the centers of mass of the respective cylinders. Both of these relative position vectors are functions of the two sets of Euler angles and Cartesian coordinates. Additional details of the characterization of the contact between the two cylinders are presented in Appendix C.

For the constraints (5.3) and (5.5) the resulting normal force direction is along $\mathbf{E}_3$ and the static friction force lies in the plane spanned by $\{\mathbf{E}_1, \mathbf{E}_2\}$. To prescribe the friction force at the contact between the two cylinders, it is also necessary to decompose the force associated with the constraint (5.9) into normal and friction components. For this, we project the constraint at the cylinders' mutual contact on the basis $\{{}_I\mathbf{e}_3, {}_{II}\mathbf{e}_3, \mathbf{n} = {}_I\mathbf{e}_3 \times {}_{II}\mathbf{e}_3/||{}_I\mathbf{e}_3 \times {}_{II}\mathbf{e}_3||\}$. The tangential (frictional) component of the contact constraint lies in the plane spanned by the basis $\{{}_I\mathbf{e}_3, {}_{II}\mathbf{e}_3\}$ while the normal component of the constraint force lies along $\mathbf{n}$. This decomposition relies on the fact that the vectors $\{{}_I\mathbf{e}_3, {}_{II}\mathbf{e}_3\}$ span the coincident tangent plane between the two cylinders at their mutual contact point.

5.2 The final set of constraints

In Appendix D, we consider the set of nine constraints (5.3), (5.5) and (5.9) for a pair of cylinders in rolling contact with each other while also in rolling contact with a horizontal surface. We find that only eight of the nine constraints are linearly independent and the system of nine constraints is not integrable. Furthermore, we demonstrate that it is very challenging to extract a set of eight linearly independent constraints from the nine constraints and equally challenging to specify a set of 8 independent Lagrange multipliers associated with rolling constraints (cf. Appendix D.2). While, it is possible to use fixed point iterations to simulate the motion of the rolling cylinders (cf. Capobianco et al. [12, Section 9]), we chose to pursue a different strategy and reexamine the contact condition between the cylinders.

Based on physical intuition, one would expect that the normal force at the contact between the two cylinders is small and thus the friction at the inter-cylinder contact point to be insufficient to prevent the two cylinders from slipping with respect to each other. The pair of rolling constraints between each cylinder and the ground (cf. (5.3) and (5.5)) and the contact condition between the two cylinders,

$$(\mathbf{v}_3 - \mathbf{v}_4) \cdot \mathbf{n} = 0, \tag{5.11}$$

amount to seven scalar constraints. We now propose an additional set of five independent constraints that will completely constrain the 12 degree-of-freedom system. As a result, we will obtain the desired motion described in Sect. 5. The five additional constraints consist of three constraints imposed on the top axis of cylinder I and two constraints imposed on the top axis of cylinder II (points P_5 and P_6 respectively in Fig. 1). We express the aforementioned constraints as follows:

$$\Pi_\Gamma = 0, \qquad (\Gamma = 1, \ldots, 12) \tag{5.12}$$

where

$$\begin{aligned}
&\Pi_1 = \mathbf{v}_1 \cdot \mathbf{E}_1, \quad \Pi_2 = \mathbf{v}_1 \cdot \mathbf{E}_2, \quad \Pi_3 = \mathbf{v}_1 \cdot \mathbf{E}_3,\\
&\Pi_4 = \mathbf{v}_2 \cdot \mathbf{E}_1, \quad \Pi_5 = \mathbf{v}_2 \cdot \mathbf{E}_2, \quad \Pi_6 = \mathbf{v}_2 \cdot \mathbf{E}_3,\\
&\Pi_7 = (\mathbf{v}_3 - \mathbf{v}_4) \cdot \mathbf{n},\\
&\Pi_8 = \mathbf{v}_5 \cdot \mathbf{E}_3, \quad \Pi_9 = \dot{\psi}_1, \quad \Pi_{10} = \dot{\varphi}_1 - \dot{\varphi}_{1_0},\\
&\Pi_{11} = \mathbf{v}_6 \cdot \mathbf{E}_3, \quad \Pi_{12} = \dot{\psi}_2.
\end{aligned} \tag{5.13}$$

Referring to Fig. 13, the constraints $\Pi_{1,2,3} = 0$ are the constraints that cylinder I rolls a single point P_1 on the horizontal surface, while the constraints $\Pi_{4,5,6} = 0$ are the constraints that cylinder II rolls with a single point P_2 on the horizontal surface. The constraint $\Pi_7 = 0$ is the contact condition for the two cylinders at the points P_3 on cylinder I and P_4 on cylinder II. To ensure that the points P_5 and P_6 only move in the horizontal direction, the constraints $\Pi_8 = 0$ and $\Pi_{11} = 0$, respectively are imposed. The constraint $\Pi_{10} = 0$ imposed on cylinder I represents the fact that the spin speed $\dot{\varphi}_1$ of cylinder I about its longitudinal axis is prescribed. Finally, the constraints $\Pi_9 = 0$ and $\Pi_{12} = 0$ combined with the other 10 constraints ensure that the centers of mass of both cylinders move in straight lines.

To enforce the constraints (5.13), constraint forces and constraint moments need to be prescribed. We use the procedure discussed in [10,18] for this purpose. The constraints $\Pi_{1,2,3} = 0$ and $\Pi_{4,5,6} = 0$ are enforced by a normal force and a static friction force acting at P_1 and P_2, respectively (cf. (D12) and (D13)). The constraint $\Pi_7 = 0$ is enforced by a normal force acting at P_3

and an equal and opposite normal force acting at P_4. Because the contact is rough, the normal forces also induce dynamic friction forces on the cylinders:

$$\begin{aligned}\mathbf{F}_{c_3} &= N_3\mathbf{n} - \mu_d\,|N_3|\,\frac{\mathbf{v}_3 - \mathbf{v}_4}{\|\mathbf{v}_3 - \mathbf{v}_4\|} \text{ acting at } P_3,\\ \mathbf{F}_{c_4} &= -\mathbf{F}_{c_3} \text{ acting at } P_4,\end{aligned} \tag{5.14}$$

where μ_d is the coefficient of dynamic friction. The constraints $\Pi_8 = 0$ and $\Pi_{11} = 0$ are enforced by forces in the $\mathbf{E}_3$ direction acting at P_5 and P_6, respectively:

$$\begin{aligned}\mathbf{F}_{c_8} &= F_8\mathbf{E}_3 \text{ acting at } P_5,\\ \mathbf{F}_{c_{11}} &= F_{11}\mathbf{E}_3 \text{ acting at } P_6.\end{aligned} \tag{5.15}$$

The constraints $\Pi_9 = 0$ and $\Pi_{10} = 0$ are enforced by pure moments acting on cylinder I and the constraint $\Pi_{12} = 0$ is enforced by a pure moment acting on cylinder II:

$$\begin{aligned}\mathbf{M}_{c_9} + \mathbf{M}_{c_{10}} &= M_{c_9\,I}\mathbf{g}^1 + M_{c_{10}\,I}\mathbf{g}^3 \text{ acting on cylinder I,}\\ \mathbf{M}_{c_{12}} &= M_{c_{12}\,II}\mathbf{g}^1 \text{ acting on cylinder II.}\end{aligned} \tag{5.16}$$

The dual Euler basis vectors (cf. (A12)) were employed to establish the representations (5.16). The constraint forces and moments associated with the constraints $\Pi_{8,9,10,11,12} = 0$ are all supplied by applied forces and moments acting on the cylinders.

6 Simulating the pair of transported cylinders

Based on our prior analysis of the possible constraints on the contacting cylinders shown in Figs. 1 and 13, we assume rolling contact of each cylinder with the horizontal surface and sliding contact at the points of mutual contact. The cylinders are supported by applied forces acting at the centers of their upper surfaces and are each given an initial spin. Thus, the system of two cylinders is subject to 12 constraints described by equation (5.13). Ignoring the occupational hazards of transporting two cylinders simultaneously in this manner, we now demonstrate that there is a mechanical advantage.

6.1 The numerical simulation method

Simulating the pair of cylinders is non-trivial. We needed to utilize Capobianco's et al. non-smooth generalized-α method for mechanical systems with frictional contact [12] to perform the simulations. The work [12] improved numerical algorithm developed by Brüls and coworkers (cf. [19–21] and references therein). These authors adopted the generalized-α algorithm to mechanical systems with bilateral constraints, non-holonomic constraints, and friction.[5] The generalized-α algorithm used in [12,19–21,24] also stabilizes the constraints at the position, velocity, and acceleration levels, thus preventing interpenetration and reducing numerical integration errors.[6]

6.2 Results from simulations

With the aid of calculations in Appendix C, we set up an initial configuration of two identical cylinders inclined at opposite angles to the vertical and touching at a single point. Motion was initiated by assigning a nonzero angular velocity to $\dot{\varphi}_{1_0}$ (cf. (5.13)), propelling cylinder I towards cylinder II. Cylinder II is driven by this motion with $\dot{\varphi}_2 = -\dot{\varphi}_{1_0}$ because both cylinders are subject to rolling constraints at their contact point with the ground. An animation of a simulation of the pair of transported cylinders using the generalized-α method can be found here: https://www.youtube.com/watch?v=61_Kfkd_s6o

Referring to (5.15) and (5.16), in addition to gravitational forces and the constraint forces at P_1, P_2, P_3, and P_4, the motions of the cylinders can be sustained by following applied forces and moments act on the cylinders:

$$\begin{aligned}{}_I\mathbf{F}_a = \mathbf{F}_{c_8} &= F_3\mathbf{E}_3 \text{ acting at } P_5,\\ \mathbf{M}_{c_9} + \mathbf{M}_{c_{10}} &= \mathbf{0} \text{ acting on cylinder I,}\\ {}_{II}\mathbf{F}_a = \mathbf{F}_{c_{11}} &= F_3\mathbf{E}_3 \text{ acting at } P_6,\\ \mathbf{M}_{c_{12}} &= \mathbf{0} \text{ acting on cylinder II.}\end{aligned} \tag{6.1}$$

[5] For additional details on the original generalized-α algorithm for structural dynamics, the reader is referred to [22,23]. The original generalized-α algorithm was used for holonomically constrained mechanical systems in the absence of friction and impacts.

[6] For additional background on constraint stabilization, the interested reader is referred to the seminal works by Baumgarte [25] and Gear, Leimkuhler, and Gupta [26].

Simulation results show that at steady state the normal force at the inter-cylinder contact is very small (on the order of the algorithm's set tolerance).[7] For example when $\vartheta = 0$ for each cylinder we have $\frac{N_1}{mg} = 0.5484$, $\frac{N_2}{mg} = 0.5484$, $\frac{N_3}{mg} = 5.9284(10^{-27})$. The result is a negligible friction force at this points of mutual contact P_3 and P_4.

Because the normal force N_3 is negligible, the dynamics of each cylinder in the pair resemble the dynamics of one cylinder that is similarly supported at its top and given a matching initial angular velocity about its longitudinal axis. This is precisely the situation analyzed in Sect. 3 and we can use our analysis of a single cylinder to examine the transport of the pair of cylinders.

6.3 Analysis of the transport mechanism

We conducted a series of simulations using two idealized large (220 ft^3) industrial high-pressure cylinders that would typically hold welding gas. The cylinders undergo the previously described motion at varying inclination angles $\vartheta_1 = \vartheta = \vartheta_2$ with respect to the vertical. For each motion the vertical force $F_3\mathbf{E}_3$ applied at the top axis of each cylinder and the normal force $N\mathbf{E}_3$ between each cylinder and the ground are displayed in Fig. 14. For the simulated, case the friction forces at the ground contact points vanished: results that is anticipated from (6.1). To verify that this case is equivalent to the case $\mu_s = 0$ discussed in Sect. 3, we superposed the curves for $\frac{N}{mg}(\vartheta)$ and $\frac{F_3}{mg}(\vartheta)$ computed using (3.10) on the results from the numerical simulations. As expected the 8 sets of results from numerical simulations lay on these curves (cf. Figure 14). The simulations show that, within a certain range of the angle ϑ, most of the weight of each cylinder is balanced by the normal force, thus enabling an efficient displacement of the cylinders as described in Sect. 1 for a range of applied forces and angles of inclination (as discussed in Sect. 3).

7 Conclusions

In this work, we analyze a transportation method for two cylindrical tanks where the cylinders are held at opposite inclinations with the vertical and touch each other at a single point point. During the motion of the cylinders, the contact points between each cylinder and the ground trace straight parallel paths.

As a preliminary work and motivated by our simulations of a pair of cylinders, we examined the optimal transport mechanisms for a single inclined rolling cylinder. In particular, we sought to determine the minimum applied force needed to support the cylinder so that it would roll on the ground while its center of mass traced a straight line at constant speed. Our calculations also considered the case where the static friction criterion was violated. Notably, we found that if an applied force $\mathbf{F}_a = F_3\mathbf{E}_3 + F\mathbf{e}$ is applied at the top of the cylinder (cf. Fig. 2), then the static friction acting at the point of contact of the cylinder with the ground facilitates a range of values of (F, F_3) to result in the rectilinear motion of the rolling cylinder for a given angle of inclination ϑ. The minimum applied force $\mathbf{F}_a$ for a given ϑ was also computed (cf. Fig. 8).

Our analysis in Sect. 4 showed that the constraints on a inclined rolling cylinder were non-integrable using two approaches: demonstrations of the holonomy of a rolling cylinder and use of the Frobenius criterion. The corresponding situation for a pair of inclined, contacting, rolling cylinders proved to be far more complex. In particular, we showed how the assumption of

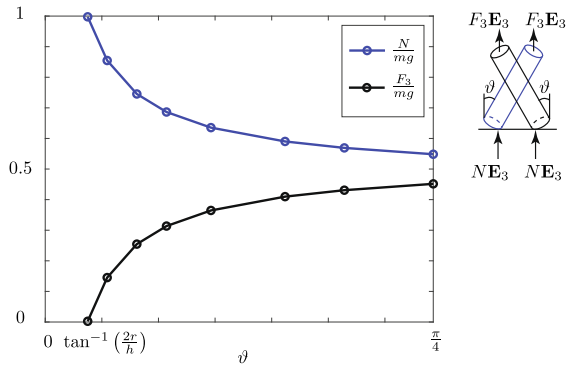

Fig. 14 The forces needed to sustain the motion of the two cylinders with dimensions $h = 1.2954$ m and $r = 0.1143$ m for several values of angle $\vartheta \in (\tan^{-1}\left(\frac{2r}{h}\right), \frac{\pi}{4})$. These forces are identical for both cylinders. The 8 sets of results in $\circ$ were obtained using numerical simulations. The friction forces on the cylinders due to their contact with the horizontal plane vanish. The curves $\frac{N}{mg}(\vartheta)$ and $\frac{F_3}{mg}(\vartheta)$ are drawn in blue and black, respectively, and are computed using (3.10). The angle $\vartheta = \tan^{-1}\left(\frac{2r}{h}\right)$ corresponds to the case where the vertical normal force on each cylinder completely balances its weight

[7] Following the notation of Capobianco et al. [12], the algorithm parameters used in this simulation are $\rho_\infty = 0.5$, $r = 0.3$, $\mathrm{TOL}_n = 1.0(10^{-8})$, $\Delta t = 0.002$ s.

rolling contact between the cylinders resulted in a set of 9 constraints only 8 of which were independent (cf. Appendix D). Moreover, finding the set of 8 independent constraints proved to be too difficult for us to solve. This analysis motivated the assumption that the contact between the cylinders was one of sliding. Our simulations of the pair of inclined cylinders rolling on a horizontal surface while in point contact (with sliding friction) showed that the normal force at the point of mutual contact was small in comparison to the other forces on the cylinders. This result enabled us to use our earlier work on a single inclined cylinder to explore the range of forces needed to transport a pair of cylinders. Static friction at the contact points with the horizontal surface enables locomotion of the cylinders for a range of applied forces: it is as simple as transporting one cylinder with the left hand and the other with the right hand.

Funding The work of Theresa Honein was supported by a graduate fellowship administered by the Department of Mechanical Engineering at the University of California, Berkeley.

Code Availibility Codes for the simulation of the cylinders and the code used to validate the Frobenius integrability criterion in Appendix D.3 can be found here: https://github.com/ThH00/On-the-Dynamics-of-Transporting-Rolling-Cylinders

Declarations

Conflict of interest The authors declare they have no conflict of interest.

Appendix A 3-1-3 Euler angle parameterization of a rotation tensor

The rotation tensors $\mathbf{Q}_1$ and $\mathbf{Q}_2$ of the individual cylinders are each parameterized by a separate set of 3-1-3 Euler angles. To provide relevant background and details, it suffices to consider a rotation tensor $\mathbf{Q}$ parameterized by a set of 3-1-3 Euler angles ψ, ϑ, and φ.

The Euler angle parameterization of $\mathbf{Q}$ can be imagined as a set of 3 compound rotations. The first rotation is defined a rotation about the $\mathbf{E}_3$ axis through a counterclockwise angle ψ. This rotation can be used to define a second basis:

$$\begin{aligned}\mathbf{e}_1' &= \cos(\psi)\mathbf{E}_1 + \sin(\psi)\mathbf{E}_2,\\ \mathbf{e}_2' &= -\sin(\psi)\mathbf{E}_1 + \cos(\psi)\mathbf{E}_2, \quad \mathbf{e}_3' = \mathbf{E}_3.\end{aligned} \tag{A1}$$

The second rotation is defined as a rotation about $\mathbf{e}_1'$ through a counterclockwise angle of rotation ϑ:

$$\begin{aligned}\mathbf{e}_1'' &= \mathbf{e}_1', \quad \mathbf{e}_2'' = \cos(\vartheta)\mathbf{e}_2' + \sin(\vartheta)\mathbf{e}_3',\\ \mathbf{e}_3'' &= -\sin(\vartheta)\mathbf{e}_2' + \cos(\vartheta)\mathbf{e}_3'.\end{aligned} \tag{A2}$$

The third and final rotation is defined as a rotation about $\mathbf{e}_3''$ through a counterclockwise angle of rotation φ:

$$\begin{aligned}\mathbf{e}_1 &= \cos(\varphi)\mathbf{e}_1'' + \sin(\varphi)\mathbf{e}_2'',\\ \mathbf{e}_2 &= -\sin(\varphi)\mathbf{e}_1'' + \cos(\varphi)\mathbf{e}_2'', \quad \mathbf{e}_3 = \mathbf{e}_3''.\end{aligned} \tag{A3}$$

That is, $\mathbf{Q} = \sum_{i=1}^{3} \mathbf{e}_i \otimes \mathbf{E}_i$ where $\otimes$ is the tensor product. The unit vectors used to define the rotations are known as the Euler basis vectors $\{\mathbf{g}_1, \mathbf{g}_2, \mathbf{g}_3\}$. For a 3-1-3 set of Euler angles:

$$\mathbf{g}_1 = \mathbf{E}_3, \qquad \mathbf{g}_2 = \mathbf{e}_1', \qquad \mathbf{g}_3 = \mathbf{e}_3. \tag{A4}$$

A discussion of the representations of the angular velocity vector can be found in [10, Section 6.8.2]:

$$\begin{aligned}\boldsymbol{\omega} &= \dot{\psi}\mathbf{E}_3 + \dot{\vartheta}\mathbf{e}_1' + \dot{\varphi}\mathbf{e}_3\\ &= \dot{\vartheta}\mathbf{e}_1'' + \dot{\psi}\cos(\vartheta)\mathbf{e}_2'' + \left(\dot{\varphi} + \dot{\psi}\cos(\vartheta)\right)\mathbf{e}_3\\ &= \left(\dot{\vartheta}\cos(\varphi) + \dot{\psi}\sin(\vartheta)\sin(\varphi)\right)\mathbf{e}_1\\ &\quad + \left(-\dot{\vartheta}\sin(\varphi) + \dot{\psi}\sin(\vartheta)\cos(\varphi)\right)\mathbf{e}_2\\ &\quad + \left(\dot{\varphi} + \dot{\psi}\cos(\vartheta)\right)\mathbf{e}_3.\end{aligned} \tag{A5}$$

The representation (A5) is very helpful when discussing instances where $\boldsymbol{\omega} \parallel \boldsymbol{\pi}_P$.

In the sequel, we will use the notation

$$\mathsf{A} = \left[\mathbf{a}\ \mathbf{b}\ \mathbf{c}\right] \tag{A6}$$

as shorthand for the matrix

$$\mathsf{A} = \begin{bmatrix} \mathbf{a}\cdot\mathbf{E}_1 & \mathbf{b}\cdot\mathbf{E}_1 & \mathbf{c}\cdot\mathbf{E}_1 \\ \mathbf{a}\cdot\mathbf{E}_2 & \mathbf{b}\cdot\mathbf{E}_2 & \mathbf{c}\cdot\mathbf{E}_2 \\ \mathbf{a}\cdot\mathbf{E}_3 & \mathbf{b}\cdot\mathbf{E}_3 & \mathbf{c}\cdot\mathbf{E}_3 \end{bmatrix}. \tag{A7}$$

For future purposes it is convenient to note that the following matrix is singular:

$$\mathsf{G} = \left[\mathbf{g}_1 \times \mathbf{x}\ \mathbf{g}_2 \times \mathbf{x}\ \mathbf{g}_3 \times \mathbf{x}\right], \tag{A8}$$

where $\mathbf{x}$ is any vector. The singular nature of G can be established by first noting that

$$\begin{aligned} \mathsf{G} &= -\left[\mathbf{x}\times\mathbf{g}_1\ \mathbf{x}\times\mathbf{g}_2\ \mathbf{x}\times\mathbf{g}_3\right] \\ &= -\left[\mathrm{Skew}(\mathbf{x})\right]\left[\mathbf{g}_1\ \mathbf{g}_2\ \mathbf{g}_3\right]. \end{aligned} \tag{A9}$$

We recall Sylvester's rank inequality, if A is an $m\times n$ matrix and B is an $n\times k$ matrix, then

$$\mathrm{rank}(\mathsf{A}) + \mathrm{rank}(\mathsf{B}) - n \le \mathrm{rank}(\mathsf{AB}). \tag{A10}$$

Knowing that $\mathrm{rank}([\mathrm{Skew}(\mathbf{x})]) = 2$, the rank inequality allows us to conclude that $\mathrm{rank}(\mathsf{G}) = 2$.

We note that the null space of G is the vector

$$\mathrm{null}(\mathsf{G}) = [\mathbf{g}_1\ \mathbf{g}_2\ \mathbf{g}_3]^{-1}\mathbf{x} = [\mathbf{g}^1\ \mathbf{g}^2\ \mathbf{g}^3]^T\mathbf{x}, \tag{A11}$$

where $\{\mathbf{g}^1\ \mathbf{g}^2\ \mathbf{g}^3\}$ is the dual Euler basis. The dual basis vectors are defined by the relations [27]

$$\mathbf{g}_k\cdot\mathbf{g}^i = 1 \text{ if } i = k \text{ and otherwise } 0. \tag{A12}$$

Thus, $\boldsymbol{\omega}\cdot\mathbf{g}^1 = \dot{\psi}$, $\boldsymbol{\omega}\cdot\mathbf{g}^2 = \dot{\vartheta}$, and $\boldsymbol{\omega}\cdot\mathbf{g}^3 = \dot{\varphi}$. Expressions for the dual basis vectors can be found in [10, Section 6.8.2]. In computing (A11), we assumed that the matrix $[\mathbf{g}_1\ \mathbf{g}_2\ \mathbf{g}_3]$ is invertible which is valid when $\vartheta \neq 0, \pi$.

Appendix B Frobenius integrability criterion applied to a rolling cylinder

The cylinder has six degrees of freedom and the motion of the rolling cylinder is subject to the three constraints $\mathbf{v}_P = \mathbf{0}$. While one of these constraints $(\mathbf{v}_P\cdot\mathbf{E}_3)$ is integrable, it is not clear if the entire system of constraints is integrable. To explore this issue, we use the Frobenius integrability criterion [28] (cf. [10,29,30]).

Each of the three constraints $\Pi_k = 0$ (cf. (2.2)) can be expressed in a canonical form $\Pi = 0$ where

$$\Pi = \mathbf{f}\cdot\bar{\mathbf{v}} + \mathbf{h}\cdot\boldsymbol{\omega}. \tag{B1}$$

After defining the 6 coordinates,

$$q^i = x_i, \quad q^4 = \psi, \quad q^5 = \vartheta, \quad q^6 = \varphi, \tag{B2}$$

where $i = 1, 2, 3$, we compute the following representations for the three constraint functions:

$$\Pi_i = \sum_{K=1}^{6} W_{iK}\dot{q}^K. \tag{B3}$$

Referring to (2.5), we find that

$$\mathsf{W} = \begin{bmatrix} 1 & 0 & 0 & \cos(\psi)\ f_1 & -\sin(\psi)\ f_2 & r\cos(\psi) \\ 0 & 1 & 0 & \sin(\psi)\ f_1 & \cos(\psi)\ f_2 & r\sin(\psi) \\ 0 & 0 & 1 & 0 & -f_1 & 0 \end{bmatrix}. \tag{B4}$$

We now define the components of three skew-symmetric matrices:

$$\begin{aligned} &S^{\Gamma}_{L,K} = \frac{\partial W_{\Gamma L}}{\partial q^K} - \frac{\partial W_{\Gamma K}}{\partial q^L}, \\ &(K, L = 1, \ldots, 6, \Gamma = 1, \ldots, 3)\,. \end{aligned} \tag{B5}$$

There remains to define three vectors:

$$\mathsf{a} = \begin{bmatrix} a_1 \\ \vdots \\ a_6 \end{bmatrix}, \quad \mathsf{b} = \begin{bmatrix} b_1 \\ \vdots \\ b_6 \end{bmatrix}, \quad \mathsf{y} = \begin{bmatrix} y_1 \\ \vdots \\ y_6 \end{bmatrix}. \tag{B6}$$

Frobenius' necessary and sufficient conditions for a system of 3 constraints, $\Pi_1 = 0, \ldots, \Pi_3 = 0$ to be integrable require the following equations to hold:

$$a^T\left(S^{\Gamma}b\right) = 0, \qquad (\Gamma = 1, \ldots, 3) \tag{B7}$$

for all values of the variables $q^1, \ldots, q^6$ and for all distinct solutions a and b to the equation

$$W\mathsf{y} = 0. \tag{B8}$$

That is, the six-dimensional vectors a and b lie in the null space of W.

To apply Frobenuis' integrability criterion, we now compute S_1, S_2, and S_3:

$$\begin{aligned}
\mathsf{S}^1 &= \begin{bmatrix} \mathsf{O}_{3\times3} & \mathsf{O}_{3\times3} \\ \mathsf{O}_{3\times3} & \mathsf{E}^1 \end{bmatrix}, \\
\mathsf{E}^1 &= \begin{bmatrix} 0 & 0 & r\sin(\psi) \\ 0 & 0 & 0 \\ -r\sin(\psi) & 0 & 0 \end{bmatrix}, \\
\mathsf{S}_2 &= \begin{bmatrix} \mathsf{O}_{3\times3} & \mathsf{O}_{3\times3} \\ \mathsf{O}_{3\times3} & \mathsf{E}^2 \end{bmatrix}, \\
\mathsf{E}^2 &= \begin{bmatrix} 0 & 0 & -r\cos(\psi) \\ 0 & 0 & 0 \\ r\cos(\psi) & 0 & 0 \end{bmatrix}, \\
\mathsf{S}_3 &= \mathsf{O}_{6\times6},
\end{aligned} \tag{B9}$$

where $\mathsf{O}_{n\times n}$ is the $n\times n$ null matrix. The 3-dimensional null space of W is spanned by the vectors

$$\mathsf{y}_1 = \begin{bmatrix} -\cos(\psi)\, f_1 \\ -\sin(\psi)\, f_1 \\ 0 \\ 1 \\ 0 \\ 0 \end{bmatrix}, \quad \mathsf{y}_2 = \begin{bmatrix} \sin(\psi)\, f_2 \\ -\cos(\psi)\, f_2 \\ f_1 \\ 0 \\ 1 \\ 0 \end{bmatrix}, \quad \mathsf{y}_3 = \begin{bmatrix} -r\cos(\psi) \\ -r\sin(\psi) \\ 0 \\ 0 \\ 0 \\ 1 \end{bmatrix}. \tag{B10}$$

Finally, applying Frobenius' criterion, we compute all unique combinations

$$\mathsf{a}^T\left(\mathsf{S}^B\mathsf{b}\right) = 0, \quad (B = 1, \ldots, 3) \tag{B11}$$

for all distinct solutions a and b of $\mathsf{W}\mathsf{y} = 0$ except for

$$\begin{aligned}
\mathsf{y}_1^T\left(\mathsf{S}^1\mathsf{y}_3\right) &= r\sin(\psi), \\
\mathsf{y}_1^T\left(\mathsf{S}^2\mathsf{y}_3\right) &= -r\cos(\psi).
\end{aligned} \tag{B12}$$

In conclusion, the application of Frobenius' criterion has while the constraint Π_3 in equation (2.2) is integrable, the system of three constraints is non-integrable.

Appendix C Contact detection between two cylinders

Given the dimensions, position, and orientation of the pair of cylinders shown in Fig. 13, we seek to determine whether the cylinders penetrate (not a valid configuration), touch at one point, or are apart from each other. This characterization of the gap distance d between the cylinders is necessary for contact detection in simulations.

For contact detection between the cylinders, we consider the following representations for the position vectors of points $\mathbf{x}_I$ and $\mathbf{x}_{II}$ of material points on the axes of the cylinders I and II, respectively:

$$\begin{aligned}
\mathbf{x}_I &= \bar{\mathbf{x}}_I + m\,{}_I\mathbf{e}_3, \\
\mathbf{x}_{II} &= \bar{\mathbf{x}}_{II} + n\,{}_{II}\mathbf{e}_3,
\end{aligned} \tag{C1}$$

where

$$m \in \left[-\frac{h_1}{2}, \frac{h_1}{2}\right] \quad \text{and} \quad n \in \left[-\frac{h_2}{2}, \frac{h_2}{2}\right] \tag{C2}$$

are coordinates. The distance between two points on the axes of the cylinders is

$$\begin{aligned}
d &= \|\mathbf{x}_{II} - \mathbf{x}_I\| \\
&= \|\bar{\mathbf{x}}_{II} + n\,{}_{II}\mathbf{e}_3 - \bar{\mathbf{x}}_I - m\,{}_I\mathbf{e}_3\|.
\end{aligned} \tag{C3}$$

We seek to find m^* and n^* corresponding to the points $\mathbf{x}_I^*$ and $\mathbf{x}_{II}^*$ for which the distance d is minimized. The relative position vectors of these points are normal to the axes of both cylinders:

$$\begin{aligned}
\left(\mathbf{x}_I^* - \mathbf{x}_{II}^*\right) \cdot {}_I\mathbf{e}_3 &= 0, \\
\left(\mathbf{x}_I^* - \mathbf{x}_{II}^*\right) \cdot {}_{II}\mathbf{e}_3 &= 0.
\end{aligned} \tag{C4}$$

With the help of (C1), we can express the pair of equations (C4) in the form

$$\mathsf{H}\mathsf{h} = \mathsf{k}, \tag{C5}$$

where

$$\mathsf{H} = \begin{bmatrix} 1 & -{}_{II}\mathbf{e}_3 \cdot {}_I\mathbf{e}_3 \\ -{}_{II}\mathbf{e}_3 \cdot {}_I\mathbf{e}_3 & 1 \end{bmatrix}, \quad \mathsf{h} = \begin{bmatrix} m^* \\ n^* \end{bmatrix}, \quad \mathsf{k} = \begin{bmatrix} (\bar{\mathbf{x}}_{II} - \bar{\mathbf{x}}_I) \cdot {}_I\mathbf{e}_3 \\ (\bar{\mathbf{x}}_I - \bar{\mathbf{x}}_{II}) \cdot {}_{II}\mathbf{e}_3 \end{bmatrix}. \tag{C6}$$

For a given configuration of the cylinders, H and k are known. We seek solutions h to the equation $\mathsf{H}\mathsf{h} = \mathsf{k}$. Notice that the matrix A is singular when the two cylinders are parallel, i.e., when ${}_{II}\mathbf{e}_3 \cdot {}_{I}\mathbf{e}_3 = \pm 1$ and there is a continuous line of contact points. In our computational algorithm to detect the contact points, we also compute the derivatives of h in order to explore what occurs at later instances of time:

$$\begin{aligned} \dot{\mathsf{h}} &= \mathsf{H}^{-1}\left(\dot{\mathsf{k}} - \dot{\mathsf{H}}\mathsf{h}\right), \\ \ddot{\mathsf{h}} &= \mathsf{H}^{-1}\left(\ddot{\mathsf{k}} - \ddot{\mathsf{H}}\mathsf{h} - 2\dot{\mathsf{H}}\dot{\mathsf{h}}\right). \end{aligned} \tag{C7}$$

If equation (C2) is satisfied by the solutions to (C5), then if

$$\begin{cases} d < r_1 + r_2 & \text{the cylinders penetrate,} \\ & \text{not a valid configuration} \\ d = r_1 + r_2 & \text{the cylinders touch,} \\ d > r_1 + r_2 & \text{the cylinders are} \\ & \text{not in contact.} \end{cases} \tag{C8}$$

Once m^* and n^* have been computed, the relative position vectors of the contact points can be found:

$$\begin{aligned} \boldsymbol{\pi}_{P_3} &= m\ {}_{I}\mathbf{e}_3 + r_1\mathbf{u}, \\ \boldsymbol{\pi}_{P_4} &= n\ {}_{II}\mathbf{e}_3 - r_2\mathbf{u}, \end{aligned} \tag{C9}$$

where the unit vector $\mathbf{u}$ is normal to the axes of both cylinders:

$$\mathbf{u} = \frac{\mathbf{x}_{II} - \mathbf{x}_I}{\|\mathbf{x}_{II} - \mathbf{x}_I\|}. \tag{C10}$$

As shown in Fig. 13, the vector $\mathbf{u} = \pm\mathbf{n}$, has the representations

$$\begin{aligned} \mathbf{u} &= \cos(\chi_1)\ {}_{I}\mathbf{e}_1 + \sin(\chi_1)\ {}_{I}\mathbf{e}_2 \\ &= \cos(\chi_2)\ {}_{II}\mathbf{e}_1 + \sin(\chi_2)\ {}_{II}\mathbf{e}_2. \end{aligned} \tag{C11}$$

In computing the solution of the contact problem and applications of the Frobenius integrability criterion, the variables m, n, χ_1, χ_2 should be considered as functions of the 12 coordinates ${}_{I}x_k$, ${}_{II}x_k$, $\psi_1, \vartheta_1, \varphi_1, \psi_2, \vartheta_2$, and φ_2.

Referring to Fig. 13, the two other contact detections of interest are the instantaneous points of contact of each cylinder with the horizontal plane: P_1 and P_4. The normal components of all three constraint velocities $\mathbf{v}_1 = \mathbf{0}, \mathbf{v}_2 = \mathbf{0}$, and $\mathbf{v}_3 - \mathbf{v}_4 = \mathbf{0}$ are holonomic.[8] Thus, we can write the gap distances for the two cylinder-ground contact and for the cylinder-cylinder contact respectively as

$$\begin{aligned} g_{N1} &= \left(\bar{\mathbf{x}}_I + \boldsymbol{\pi}_{P_1}\right) \cdot \mathbf{E}_3, \\ g_{N2} &= \left(\bar{\mathbf{x}}_{II} + \boldsymbol{\pi}_{P_2}\right) \cdot \mathbf{E}_3, \\ g_{N3} &= \|\mathbf{x}_3 - \mathbf{x}_4\| - (r_1 + r_2) \\ &= (\mathbf{x}_3 - \mathbf{x}_4) \cdot \mathbf{n} - (r_1 + r_2). \end{aligned} \tag{C12}$$

Appendix D Frobenius integrability criterion applied to a pair of rolling cylinders

We now consider a pair of cylinders each of which rolls with one point in contact with a horizontal surface. The cylinders are also in mutual contact at a single point. Our interest lies in the case where there is sufficient static friction such that the contact between the cylinders is also one of rolling. Referring to (5.3), (5.5), and (5.9), the system is subject to 9 constraints:

$$\Pi_\Gamma = 0, \qquad (\Gamma = 0, \ldots, 9), \tag{D1}$$

where

$$\begin{aligned} \Pi_k &= \mathbf{v}_1 \cdot \mathbf{E}_k, \quad (k = 1, 2, 3), \\ \Pi_{k+3} &= \mathbf{v}_2 \cdot \mathbf{E}_k, \\ \Pi_{k+6} &= (\mathbf{v}_3 - \mathbf{v}_4) \cdot \mathbf{E}_k. \end{aligned} \tag{D2}$$

The cylinder has six degrees of freedom and the motion of the rolling cylinder is subject to the three constraints $\mathbf{v}_P = \mathbf{0}$. While one of these constraints $(\mathbf{v}_P \cdot \mathbf{E}_3)$ is integrable, it is not clear if the entire system of constraints is integrable. To explore this issue, we use the Frobenius integrability criterion [28] (cf. [10,29,30]).

[8] According to Papastavridis [11, Section 2.2 p. 249] every condition expressing the direct contact of two rigid bodies, or the contact of one of its bodies with a foreign obstacle (environment) that is either fixed or has known motion (i.e., its position coordinates are known functions of time only), results in a holonomic equation of motion, and the corresponding contact forces are the reactions of that constraint.

D.1 Expressions for the constraint matrix W

We recall the definitions for the 12 coordinates:

$$\begin{aligned} &q^i = x_{I_i}, \quad q^4 = \psi_1, \quad q^5 = \vartheta_1, \quad q^6 = \varphi_1, \\ &q^{i+6} = x_{II_i}, \quad q^{10} = \psi_2, \quad q^{11} = \vartheta_2, \quad q^{12} = \varphi_2, \end{aligned} \tag{D3}$$

where $i = 1, 2, 3$. Each of the constraint functions Π_Γ in (D2) are linear functions of the velocities:

$$\Pi_\Gamma = \sum_{K=1}^{12} W_{\Gamma_K} \dot{q}^K. \tag{D4}$$

With some additional work, we find that the matrix W has the following block structure:

$$\mathsf{W} = \begin{bmatrix} W_{1_1} & \dots & W_{1_{12}} \\ \vdots & & \vdots \\ W_{9_1} & \dots & W_{9_{12}} \end{bmatrix} = \begin{bmatrix} \mathsf{I}_{3\times3} & \mathsf{A} & \mathsf{O}_{3\times3} & \mathsf{O}_{3\times3} \\ \mathsf{O}_{3\times3} & \mathsf{O}_{3\times3} & \mathsf{I}_{3\times3} & \mathsf{B} \\ \mathsf{I}_{3\times3} & \mathsf{C} & -\mathsf{I}_{3\times3} & -\mathsf{D} \end{bmatrix}. \tag{D5}$$

In the expression for the matrix W, $\mathsf{I}_{3\times3}$ is the 3×3 identity matrix and

$$\begin{aligned} \mathsf{A} &= \left[\mathbf{E}_3 \times \boldsymbol{\pi}_{P_1}\ {}_I\mathbf{e}_1' \times \boldsymbol{\pi}_{P_1}\ {}_I\mathbf{e}_3 \times \boldsymbol{\pi}_{P_1}\right] \\ &= \begin{bmatrix} -\boldsymbol{\pi}_{P_1} \cdot \mathbf{E}_2 & \left(\boldsymbol{\pi}_{P_1} \cdot \mathbf{E}_3\right)\sin(\psi_1) & -r_1\cos(\psi_1) \\ \boldsymbol{\pi}_{P_1} \cdot \mathbf{E}_1 & -\left(\boldsymbol{\pi}_{P_1} \cdot \mathbf{E}_3\right)\cos(\psi_1) & -r_1\sin(\psi_1) \\ 0 & \boldsymbol{\pi}_{P_1} \cdot {}_I\mathbf{e}_2' & 0 \end{bmatrix}, \\ \mathsf{B} &= \left[\mathbf{E}_3 \times \boldsymbol{\pi}_{P_2}\ {}_{II}\mathbf{e}_1' \times \boldsymbol{\pi}_{P_2}\ {}_{II}\mathbf{e}_3 \times \boldsymbol{\pi}_{P_2}\right], \\ \mathsf{C} &= \left[\mathbf{E}_3 \times \boldsymbol{\pi}_{P_3}\ {}_I\mathbf{e}_1' \times \boldsymbol{\pi}_{P_3}\ {}_I\mathbf{e}_3 \times \boldsymbol{\pi}_{P_3}\right], \\ \mathsf{D} &= \left[\mathbf{E}_3 \times \boldsymbol{\pi}_{P_4}\ {}_{II}\mathbf{e}_1' \times \boldsymbol{\pi}_{P_4}\ {}_{II}\mathbf{e}_3 \times \boldsymbol{\pi}_{P_4}\right]. \end{aligned} \tag{D6}$$

Observe that each of the matrices A, B, C, D, and their linear combinations are of the form (A8) and are thus singular. To determine the rank of W, we perform the following matrix row manipulations.

$$\mathsf{W} = \begin{bmatrix} \mathsf{I} & \mathsf{A} & 0 & 0 \\ 0 & 0 & \mathsf{I} & \mathsf{B} \\ \mathsf{I} & \mathsf{C} & -\mathsf{I} & -\mathsf{D} \end{bmatrix} \rightarrow \begin{bmatrix} \mathsf{I} & \mathsf{A} & 0 & 0 \\ 0 & 0 & \mathsf{I} & \mathsf{B} \\ 0 & \mathsf{C}-\mathsf{A} & 0 & \mathsf{B}-\mathsf{D} \end{bmatrix}, \tag{D7}$$

and observe that $\mathsf{C} - \mathsf{A}$ and $\mathsf{B} - \mathsf{D}$ are also of the form of equation (A8). The rows of $[0\ \mathsf{C}-\mathsf{A}\ 0\ \mathsf{B}-\mathsf{D}]$ can be manipulated in a similar manner to show that the rank of $[0\ \mathsf{C} - \mathsf{A}\ 0\ \mathsf{B} - \mathsf{D}]$ is 2 and thus the rank of W is 8. We conclude from this result that only eight of the nine constraints $\Pi_1 = 0, \dots, \Pi_9 = 0$ are independent.

We note that in the singular case where $\mathsf{C} - \mathsf{A} = 0$ and $\mathsf{B} - \mathsf{D} = 0$ corresponding to the case when the contact points between the two cylinders coincide with the contact points of each cylinder with the ground, rank(W) reduces to 6.

The null space of W is spanned by the vector w_n:

$$\mathsf{w}_n = \begin{bmatrix} -\mathsf{A}\mathsf{y} \\ \mathsf{y} \\ -\mathsf{B}\mathsf{z} \\ \mathsf{z} \end{bmatrix}, \tag{D8}$$

where $\mathsf{y} = [y_1, y_2, y_3]^T$ and $\mathsf{z} = [z_1, z_2, z_3]^T$ are 3-dimensional arrays whose components satisfy the identity

$$(\mathsf{C} - \mathsf{A})\,\mathsf{y} + (\mathsf{D} - \mathsf{B})\,\mathsf{z} = 0. \tag{D9}$$

With the assistance of (A9) and (A11), we obtain the following solutions to equation (D9):

$$\begin{aligned} \mathsf{y} &= [{}_I\mathbf{g}^1\ {}_I\mathbf{g}^2\ {}_I\mathbf{g}^3]^T[\boldsymbol{\pi}_{P_2} - \boldsymbol{\pi}_{P_4}], \\ \mathsf{z} &= [{}_{II}\mathbf{g}^1\ {}_{II}\mathbf{g}^2\ {}_{II}\mathbf{g}^3]^T[\boldsymbol{\pi}_{P_1} - \boldsymbol{\pi}_{P_3}]. \end{aligned} \tag{D10}$$

The resulting expression for (D8),

$$\mathsf{w}_n = \begin{bmatrix} [\boldsymbol{\pi}_{P_1} \times (\boldsymbol{\pi}_{P_2} - \boldsymbol{\pi}_{P_4})] \\ [{}_I\mathbf{g}^1\ {}_I\mathbf{g}^2\ {}_I\mathbf{g}^3]^T[\boldsymbol{\pi}_{P_2} - \boldsymbol{\pi}_{P_4}] \\ [\boldsymbol{\pi}_{P_2} \times (\boldsymbol{\pi}_{P_1} - \boldsymbol{\pi}_{P_3})] \\ [{}_{II}\mathbf{g}^1\ {}_{II}\mathbf{g}^2\ {}_{II}\mathbf{g}^3]^T[\boldsymbol{\pi}_{P_1} - \boldsymbol{\pi}_{P_3}] \end{bmatrix}, \tag{D11}$$

has no obvious interpretation. As a result, it is challenging to reduce the nine constraint equations (D1) to a single set of eight independent constraints.

D.2 Comments on constraint forces

The constraint forces and constraint moments associated with the nine constraints can be prescribed using a standard procedure (cf. [10,18]). Thus, the constraints at P_1 will be enforced by a pair of static Coulomb friction forces and a normal force acting at P_1:

$$\mathbf{F}_{c_1} = F_{f_1}\mathbf{E}_1 + F_{f_2}\mathbf{E}_2 + N_1\mathbf{E}_3 \text{ acting at } P_1. \tag{D12}$$

Similarly, the constraints at P_2 will be enforced by a pair of static Coulomb friction forces and a normal force acting at P_2:

$$\mathbf{F}_{c_2} = F_{f_3}\mathbf{E}_1 + F_{f_4}\mathbf{E}_2 + N_2\mathbf{E}_3 \text{ acting at } P_2. \quad \text{(D13)}$$

For the mutual contact, the constraints are enforced by the following set of friction and normal forces:

$$\begin{aligned} &\mathbf{F}_{c_3} = F_{f_5 I}\mathbf{e}_3 + F_{f_6 II}\mathbf{e}_3 + N_3\mathbf{n} \text{ acting at } P_3, \\ &\mathbf{F}_{c_4} = -\mathbf{F}_{c_3} \text{ acting at } P_4. \end{aligned} \quad \text{(D14)}$$

The components $F_{f_1}, \ldots F_{f_6}$, N_1, N_2, and N_3 can be considered as Lagrange multipliers enforcing the nine constraints $\Pi_1 = 0, \ldots, \Pi_9 = 0$. However, because these constraints are not independent, one of the multipliers is redundant. Determining the redundant multiplier is non-trivial.

D.3 Expressions for the skew–symmetric matrices S^Γ

We recall from (B5) that a set of 9 skew-symmetric matrices S^Γ need to be examined. The components of S^Γ have the following representation:

$$\begin{aligned} &S^\Gamma_{L,K} = \frac{\partial W_{\Gamma_L}}{\partial q^K} - \frac{\partial W_{\Gamma_K}}{\partial q^L}, \\ &(K, L = 1, \ldots, 12, \Gamma = 1, \ldots, 9)\,. \end{aligned} \quad \text{(D15)}$$

Four of the nine skew-symmetric matrices have only one distinct element and two of the matrices are identically zero:

$$\mathsf{S}^1 = \begin{bmatrix} \mathsf{O}_{3\times3} & \mathsf{O}_{3\times3} & \mathsf{O}_{3\times3} & \mathsf{O}_{3\times3} \\ \mathsf{O}_{3\times3} & -\mathsf{E}^1 & \mathsf{O}_{3\times3} & \mathsf{O}_{3\times3} \\ \mathsf{O}_{3\times3} & \mathsf{O}_{3\times3} & \mathsf{O}_{3\times3} & \mathsf{O}_{3\times3} \\ \mathsf{O}_{3\times3} & \mathsf{O}_{3\times3} & \mathsf{O}_{3\times3} & \mathsf{O}_{3\times3} \end{bmatrix},$$

$$\mathsf{E}^1 = \begin{bmatrix} 0 & 0 & r_1 \sin({}_I\psi) \\ 0 & 0 & 0 \\ -r_1 \sin({}_I\psi) & 0 & 0 \end{bmatrix}, \quad \text{(D16)}$$

$$\mathsf{S}^2 = \begin{bmatrix} \mathsf{O}_{3\times3} & \mathsf{O}_{3\times3} & \mathsf{O}_{3\times3} & \mathsf{O}_{3\times3} \\ \mathsf{O}_{3\times3} & -\mathsf{E}^2 & \mathsf{O}_{3\times3} & \mathsf{O}_{3\times3} \\ \mathsf{O}_{3\times3} & \mathsf{O}_{3\times3} & \mathsf{O}_{3\times3} & \mathsf{O}_{3\times3} \\ \mathsf{O}_{3\times3} & \mathsf{O}_{3\times3} & \mathsf{O}_{3\times3} & \mathsf{O}_{3\times3} \end{bmatrix},$$

$$\mathsf{E}^2 = \begin{bmatrix} 0 & 0 & -r_1 \cos({}_I\psi) \\ 0 & 0 & 0 \\ r_1 \cos({}_I\psi) & 0 & 0 \end{bmatrix}, \quad \text{(D17)}$$

$$\mathsf{S}^3 = \mathsf{O}_{12\times12}, \quad \text{(D18)}$$

and

$$\mathsf{S}^4 = \begin{bmatrix} \mathsf{O}_{3\times3} & \mathsf{O}_{3\times3} & \mathsf{O}_{3\times3} & \mathsf{O}_{3\times3} \\ \mathsf{O}_{3\times3} & \mathsf{O}_{3\times3} & \mathsf{O}_{3\times3} & \mathsf{O}_{3\times3} \\ \mathsf{O}_{3\times3} & \mathsf{O}_{3\times3} & \mathsf{O}_{3\times3} & \mathsf{O}_{3\times3} \\ \mathsf{O}_{3\times3} & \mathsf{O}_{3\times3} & \mathsf{O}_{3\times3} & \mathsf{F}^4 \end{bmatrix},$$

$$\mathsf{F}^4 = \begin{bmatrix} 0 & 0 & r_2 \sin({}_{II}\psi) \\ 0 & 0 & 0 \\ -r_2 \sin({}_{II}\psi) & 0 & 0 \end{bmatrix}, \quad \text{(D19)}$$

$$\mathsf{S}^5 = \begin{bmatrix} \mathsf{O}_{3\times3} & \mathsf{O}_{3\times3} & \mathsf{O}_{3\times3} & \mathsf{O}_{3\times3} \\ \mathsf{O}_{3\times3} & \mathsf{O}_{3\times3} & \mathsf{O}_{3\times3} & \mathsf{O}_{3\times3} \\ \mathsf{O}_{3\times3} & \mathsf{O}_{3\times3} & \mathsf{O}_{3\times3} & \mathsf{O}_{3\times3} \\ \mathsf{O}_{3\times3} & \mathsf{O}_{3\times3} & \mathsf{O}_{3\times3} & \mathsf{F}^5 \end{bmatrix},$$

$$\mathsf{F}^5 = \begin{bmatrix} 0 & 0 & -r_2 \cos({}_{II}\psi) \\ 0 & 0 & 0 \\ r_2 \cos({}_{II}\psi) & 0 & 0 \end{bmatrix}, \quad \text{(D20)}$$

$$\mathsf{S}^6 = \mathsf{O}_{12\times12}. \quad \text{(D21)}$$

The matrix S^3 and components W_{3_L} are associated with the integrable constraint $\mathbf{v}_{P_1} \cdot \mathbf{E}_3 = 0$:

$$\frac{d}{dt}\left({}_I x_3 - r_1 \sin({}_I\vartheta) - \frac{h_1}{2}\cos({}_I\vartheta)\right) = 0. \quad \text{(D22)}$$

Similarly, the matrix S^6 and components W_{6_L} are associated with the integrable constraint $\mathbf{v}_{P_2} \cdot \mathbf{E}_3 = 0$:

$$\frac{d}{dt}\left({}_{II} x_3 - r_2 \sin({}_{II}\vartheta) - \frac{h_2}{2}\cos({}_{II}\vartheta)\right) = 0. \quad \text{(D23)}$$

The remaining three matrices $\mathsf{S}^{7,8,9}$ are far more complicated because the coordinates m, n, and $\chi_{1,2}$ (cf. (C9)) are non-trivial functions of $q^1, \ldots, q^{12}$:

$$\mathsf{S}^\Gamma = \begin{bmatrix} \mathsf{M}^\Gamma & \mathsf{E}^\Gamma & \mathsf{N}^\Gamma & \mathsf{F}^\Gamma \\ -\mathsf{E}^\Gamma & \mathsf{G}^\Gamma & \mathsf{H}^\Gamma & \mathsf{I}^\Gamma \\ -\mathsf{N}^\Gamma & -\mathsf{H}^\Gamma & \mathsf{J}^\Gamma & \mathsf{K}^\Gamma \\ -\mathsf{F}^\Gamma & -\mathsf{I}^\Gamma & -\mathsf{K}^\Gamma & \mathsf{L}^\Gamma \end{bmatrix}, \quad \text{(D24)}$$

where $\Gamma = 7, 8, 9$ and each of the 3×3 matrices $\mathsf{E}^\Gamma, \ldots \mathsf{M}^\Gamma$ are skew-symmetric. A Matlab code that calculates the expressions S^Γ for $\Gamma = 7, 8, 9$ is available with the supplementary materials. The expressions of S^Γ for $\Gamma = 7, 8, 9$ are complicated, so calculating

$\mathsf{a}^T\left(\mathsf{S}^B\mathsf{b}\right)$ $(B = 7, \ldots 9)$ for all 12-dimensional distinct solutions a and b of $\mathsf{W}\mathsf{y} = 0$ (cf. (B7)) symbolically is not straightforward. However, we verify using a numerical example[9] that equations $\mathsf{a}^T\left(\mathsf{S}^B\mathsf{b}\right) \neq 0$ for all possible a and b. In conclusion, the system of nine constraints (D1) is not integrable.

References

1. Appell, P.: Sur l'intégration des équations du mouvement d'un corps pesant de révolution roulant par une arête circulaire sur un plan horizontal. Rendiconti del Circolo Matematico di Palermo **14**, 1–6 (1900). https://doi.org/10.1007/BF03012823
2. Korteweg, D.J.: Extrait d'une lettre à M. Appell. Rendiconti del Circolo Mathematico di Palermo **14**, 7–8 (1900). https://doi.org/10.1007/BF03012824
3. Batista, M.: Steady motion of a rigid disk of finite thickness on a horizontal plane. Int. J. Non-Linear Mech. **41**(4), 605–621 (2006). https://doi.org/10.1016/j.ijnonlinmec.2006.02.005
4. Borisov, A.V., Mamaev, I.S.: Conservation laws, hierarchy of dynamics and explicit integration of nonholonomic systems. Regular Chaotic Dyn. **13**(5), 443–490 (2008). https://doi.org/10.1134/S1560354708050079
5. Kessler, P., O'Reilly, O.M.: The ringing of Euler's disk. Regular Chaotic Dyn. **7**(1), 49–60 (2002). https://doi.org/10.1070/RD2002v007n01ABEH000195
6. Srinivasan, M., Ruina, A.: Rocking and rolling: a can that appears to rock might actually roll. Phys. Rev. **E78**, 066609 (2008). https://doi.org/10.1103/PhysRevE.78.066609
7. Bryant, R.L.: Geometry of manifolds with special holonomy: "100 years of holonomy". In: 150 Years of Mathematics at Washington University in St. Louis. Contemporary Mathematics, vol. 395, pp. 29–38. American Mathematical Society, Providence, RI (2006). https://doi.org/10.1090/conm/395/07414
8. Johnson, B.D.: The nonholonomy of the rolling sphere. Am. Math. Mon. **200**(6), 500–508 (2007)
9. Honein, T.E., O'Reilly, O.M.: Explorations of the holonomy of a rolling sphere. Proc. R. Soc. A **480**(2282), 20230684 (2024). https://doi.org/10.1098/rspa.2023.0684
10. O'Reilly, O.M.: Intermediate Dynamics for Engineers: Newton-Euler and Lagrangian Mechanics, 2nd edn. Cambridge University Press, Cambridge (2020). https://doi.org/10.1017/9781108644297
11. Papastavridis, J.G.: Analytical Mechanics: A Comprehensive Treatise on the Dynamics of Constrained Systems, Reprint edn. World Scientific, Singapore (2014). https://doi.org/10.1142/8058
12. Capobianco, G., Harsch, J., Eugster, S.R., Leine, R.I.: A nonsmooth generalized-alpha method for mechanical systems with frictional contact. Int. J. Num. Methods Eng. **122**(22), 6497–6526 (2021). https://doi.org/10.1002/nme.6801
13. Shuster, M.D.: A survey of attitude representations. J Astronaut. Sci. **41**(4), 439–517 (1993)
14. Hemingway, E.G., O'Reilly, O.M.: Perspectives on Euler angle singularities, gimbal lock, and the orthogonality of applied forces and applied moments. Multibody Syst. Dyn. **44**(1), 31–56 (2018). https://doi.org/10.1007/s11044-018-9620-0
15. Burke, W.L.: Applied Differential Geometry. Cambridge University Press, Cambridge (1985). https://doi.org/10.1017/CBO9781139171786
16. Nelson, E.: Tensor Analysis. Princeton University Press, Princeton, New Jersey (1967)
17. O'Reilly, O.M.: The dynamics of rolling disks and sliding disks. Nonlinear Dyn. **10**(3), 287–305 (1996). https://doi.org/10.1007/BF00045108
18. O'Reilly, O.M., Srinivasa, A.R.: A simple treatment of constraint forces and constraint moments in the dynamics of rigid bodies. ASME Appl. Mech. Rev. **67**(1), 014801–0148018 (2014)
19. Arnold, M., Brüls, O.: Convergence of the generalized-alpha scheme for constrained mechanical systems. Multibody Syst. Dyn. **18**, 185–202 (2007). https://doi.org/10.1007/s11044-007-9084-0
20. Brüls, O., Cardona, A., Arnold, M.: Lie group generalized-time integration of constrained flexible multibody systems. Mech. Mach. Theor. **48**, 121–137 (2012). https://doi.org/10.1007/s11044-007-9084-0
21. Cosimo, A., Galvez, J., Cavalieri, F.J., Cardona, A., Brüls, O.: A robust nonsmooth generalized-alpha scheme for flexible systems with impacts. Multibody Syst. Dyn. **48**, 127–149 (2020). https://doi.org/10.1007/s11044-019-09692-2
22. Chung, J., Hulbert, G.M.: A time integration algorithm for structural dynamics with improved numerical dissipation: the generalized-α method. ASME J. Appl. Mech. **60**(2), 371–375 (1993). https://doi.org/10.1115/1.2900803
23. Erlicher, S., Bonaventura, L., Bursi, O.: The analysis of the generalized-α method for non-linear dynamic problems. Comput. Mech. **28**, 83–104 (2002). https://doi.org/10.1007/s00466-001-0273-z
24. Brüls, O., Acary, V., Cardona, A.: Simultaneous enforcement of constraints at position and velocity levels in the nonsmooth generalized-alpha scheme. Comput. Methods Appl. Mech. Eng. **281**, 131–161 (2014). https://doi.org/10.1016/j.cma.2014.07.025
25. Baumgarte, J.: Stabilization of constraints and integrals of motion in dynamical systems. Comput. Methods Appl. Mech. Eng. **1**(1), 1–16 (1972). https://doi.org/10.1016/0045-7825(72)90018-7
26. Gear, C.W., Leimkuhler, B., Gupta, G.K.: Automatic integration of Euler-Lagrange equations with constraints. J. Comput. Appl. Math. **12**, 77–90 (1985). https://doi.org/10.1016/0377-0427(85)90008-1
27. O'Reilly, O.M.: The dual Euler basis: constraints, potentials, and Lagrange's equations in rigid body dynamics. ASME J. Appl. Mech. **74**(2), 256–258 (2007). https://doi.org/10.1115/1.2190231
28. Frobenius, G.: Ueber das Pfaffsche problem. Crelles Journal für die reine und angewandte Mathematik **82**, 230–315 (1877). https://doi.org/10.1515/crll.1877.82.230

[9] The computations can be found in the supplemental materials.

29. Forsyth, A.R.: Theory of Differential Equations. Cambridge University Press, London (1890)
30. Hawkins, T.: Frobenius, Cartan, and the problem of Pfaff. Arch. Hist. Exact Sci. **59**(4), 381–436 (2005). https://doi.org/10.1007/s00407-004-0095-4